Stem Cell Reports
Article

ISSCR

OPEN ACCESS

Healing of a Large Long-Bone Defect through Serum-Free In Vitro Priming of Human Periosteum-Derived Cells

Johanna Bolander,[1,2] Wei Ji,[1,2] Jeroen Leijten,[1,2,3] Liliana Moreira Teixeira,[1,2] Veerle Bloemen,[2,4] Dennis Lambrechts,[1,2] Malay Chaklader,[1,2] and Frank P. Luyten[1,2,*]

[1]Tissue Engineering Laboratory, Skeletal Biology and Engineering Research Center
[2]Prometheus, Division of Skeletal Tissue Engineering
KU Leuven, O&N 1, Herestraat 49, Box 813 13, 3000 Leuven, Belgium
[3]Department of Developmental BioEngineering, MIRA Institute for Biomedical Technology and Technical Medicine, University of Twente, Drienerlolaan 5, 7522NB Enschede, the Netherlands
[4]Materials Technology TC, Campus Group T, KU Leuven, Andreas Vesaliusstraat 13, 3000 Leuven, Belgium
*Correspondence: frank.luyten@uzleuven.be
http://dx.doi.org/10.1016/j.stemcr.2017.01.005

SUMMARY

Clinical translation of cell-based strategies for regenerative medicine demands predictable in vivo performance where the use of sera during in vitro preparation inherently limits the efficacy and reproducibility. Here, we present a bioinspired approach by serum-free pre-conditioning of human periosteum-derived cells, followed by their assembly into microaggregates simultaneously primed with bone morphogenetic protein 2 (BMP-2). Pre-conditioning resulted in a more potent progenitor cell population, while aggregation induced osteochondrogenic differentiation, further enhanced by BMP-2 stimulation. Ectopic implantation displayed a cascade of events that closely resembled the natural endochondral process resulting in bone ossicle formation. Assessment in a critical size long-bone defect in immunodeficient mice demonstrated successful bridging of the defect within 4 weeks, with active contribution of the implanted cells. In short, the presented serum-free process represents a biomimetic strategy, resulting in a cartilage tissue intermediate that, upon implantation, robustly leads to the healing of a large long-bone defect.

INTRODUCTION

Cell-based advanced therapy medicinal products (ATMPs) have the potential to transform our health care systems, especially for patients with failing intrinsic tissue regeneration such as complex and large bone defects in compromised biological conditions (Einhorn and Gerstenfeld, 2015). The standard approach of this strategy typically includes: (1) donor cells to form tissues together with available host cells, (2) stimulatory factors to direct cellular processes, and (3) biomaterials to provide cells with 3D cues (Leijten and Khademhosseini, 2016). Despite major advances in the design, production and in vitro performance of ATMPs, only a fraction displays suitable characteristics for clinical translation (Leijten et al., 2014). Major reasons for this lack in clinical monetization of research efforts can be attributed to a poor design and lack of robust manufacturing protocols. In terms of the design, a biomimetic strategy inspired by developmental embryology provides a scientific foundation and offers key clues regarding the main players, sequences of events and 3D stimulatory cues in postnatal fracture healing (Lenas et al., 2009; Ingber et al., 2006; Ueno et al., 2001; Knothe Tate et al., 2008). Previous reports established that large bone defects mainly heal through the formation of an intermediate cartilaginous callus (Einhorn and Gerstenfeld, 2015). Consequently, in order to mimic the native healing process of a large long-bone defect, a cell-based ATMP was designed to develop along the endochondral route. However, the classical cell source for bone repair used today is a bone marrow aspirate from the iliac crest. Yet, bone marrow-derived cells exclusively contribute to fracture healing by direct bone formation (Colnot, 2009). In consequence, periosteum-derived cells (PDCs), the main contributing cells in endochondral fracture healing, may be a more clinically relevant cell source (Colnot, 2009; Colnot et al., 2012). Moreover, PDCs have shown osteochondrogenic potential both in vitro and in vivo (De Bari et al., 2006). As stimulatory factors, bone morphogenetic proteins (BMPs) are of relevance due to their crucial role in PDC-mediated fracture healing (Tsuji et al., 2006; Chappuis et al., 2012). Moreover, specific BMP ligands have been shown to induce human PDC (hPDC)-mediated ectopic ossicle formation (Bolander et al., 2016).

Approval for clinical applications of BMP-2 and BMP-7 has already been obtained. However, their use has been associated with unpredictable bone formation due to a number of reasons, including the delivery of the supraphysiological levels required for progenitor cell recruitment (Shields et al., 2006; Pobloth et al., 2015). In vitro primed cell-based ATMPs could overcome this hurdle by delivery of the crucial number of progenitors required, appropriately primed in vitro to regenerate the damaged tissue in vivo. However, until now, in vitro stimulation of progenitor cells for in vivo tissue regeneration has been challenging. Long-term in vitro stimulated cells often fail to

integrate with the host, likely due to the maturity of the tissue (Yamashita et al., 2015). Shorter priming periods on the other hand, seem not to be sufficient in terms of clinically relevant results (Eyckmans et al., 2013). A potential reason for this can be that the in vitro priming is carried out in medium containing serum (Ryan, 1979). Indeed, serum contains an undefined and variable range of factors such as cytokines and inhibitors that bind to cell surface receptors. In consequence, batch-to-batch variability significantly affects the characteristics of cell-based implants, leading to unpredictable behavior and outcomes (Jung et al., 2012; Baker, 2016).

It was therefore hypothesized that serum-free pre-conditioning of hPDCs prior to growth factor treatment could improve the cellular response. A chemically defined serum-free pre-conditioning regime of hPDCs was developed that led to an adapted progenitor cell population with improved differentiation capacity. When assembling the pre-conditioned cells into microaggregates, mimicking cellular condensations by providing biomimetic 3D cues, and simultaneously treating them with BMP-2, cell specification toward the osteochondrogenic lineages was observed. Interestingly, physiologically relevant levels of autocrine and paracrine growth factors were secreted by the fate-steered, engineered microtissues. In vivo, the self-sustained implant proceeded to mature into endochondral bone, recapitulating long-bone fracture healing. We anticipate that the proposed serum-free strategy can be translated in a wide array of applications within the field of regenerative medicine.

RESULTS

Pre-conditioning Induces a Cellular Identity Shift toward a CD34$^+$ Progenitor

To define the culture conditions that maintained cell viability without enhancing proliferation, hPDCs were cultured for 6 days in a chemically defined medium (CDM) and compared with hPDCs cultured in growth medium (GM) containing 10% fetal bovine serum. After 24 hr, as well as after 6 days of culture, cells in CDM showed no cell proliferation compared with GM-cultured cells (Figure 1A). However, after 6 days, elevated DNA contents per cell were seen in pre-conditioned cells (Figure 1B). To investigate whether adaptations in the cell cycle were caused, expression levels of cell cycle markers cyclin-dependent kinase 1 (*CDK1*), cyclin E1 (*CCNE1*), and baculoviral inhibitor of apoptosis repeat-containing 5 (*BIRC5*) were determined. Expression of *CDK1*, essential for cell cycle progression during S and G2 phases, displayed a 6-fold upregulation in pre-conditioned cells (Figure 1C). Similarly, a 7-fold increased transcript level of *CCNE1*, required for G1/S transition was found (Figure 1D). Interestingly, a 10-fold increased level of *BIRC5*, a negative regulator of apoptosis during the G2/M phase was also seen in pre-conditioned cells (Figure 1E). To further investigate changes in cellular identity, flow cytometry was performed to characterize the expression of conventional mesenchymal stem cell markers (Figure 1F). It was shown that over 97% of cells grown in GM were positive for CD73, CD90, and CD105, whereas only 81% of cells cultured in CDM were positive for CD105. Cells from both conditions were negative for CD14, CD20, and CD45 (Figure S1A), but 70% of the CDM pre-conditioned cells displayed positivity for CD34 (Figure 1F), a phenomenon that was not seen in human bone marrow stromal cells (Figure S1B). Kinetic studies by mRNA transcript analysis and flow cytometry revealed a gradual increase in *CD34* expression as well as in the amount of receptors per cell during pre-conditioning (Figures 1G and 1H). The opposite trend was seen for CD105, where pre-conditioning led to a decreased expression of *CD105* cells as well as a reduced amount of receptors per cell (Figures 1I and 1J). Of note, mRNA transcript levels of *CD34* displayed a 70- and 20-fold higher expression in hPDCs from individual donors at passage zero (p0) compared with GM-expanded cells at passage 6 (p6), respectively (Figure S1C). In addition, CDM pre-conditioning led to increased cell size and less granularity (Figure S1D). However, no significant aberrations were observed in karyotype analysis (Figure S1E).

To investigate whether the pre-conditioning regimen may lead to an enhanced BMP response, mRNA transcript analysis of BMP type 1 and type 2 receptors was performed. CDM pre-conditioned cells displayed an increased expression of BMP type 1 (*ALK1*, *ALK2*, *ALK3*, and *ALK6*) and type 2 (*BMPR2*, *ACVR2a*, and *ACVR2b*) receptors, in comparison with standard cultured cells (Figure 1K). To further characterize the CDM-grown cells, mRNA transcript analysis displayed elevated expression of secreted factors relevant to bone formation: a 10-, 12-, and 4.6-fold increase for basic fibroblast growth factor (*FGF-2*), vascular endothelial growth factor (*VEGF*), and matrix metallopeptidase 9 (*MMP9*) expression, respectively (Figure 1L). These results were also confirmed on the protein level through an ELISA assay on conditioned medium (Figure 1M). Combined, these data indicate that the serum-free pre-conditioning led to an adapted cellular phenotype specific for hPDCs. Reduced positivity for MSC markers was correlated to increased positivity for CD34 and elevated expression of BMP receptors, identifying a switch in cellular identity.

Enhanced Effect of BMP-2-Induced Differentiation in Pre-conditioned hPDCs

Next, we set out to investigate whether these changes would translate into distinct responses upon BMP treatment.

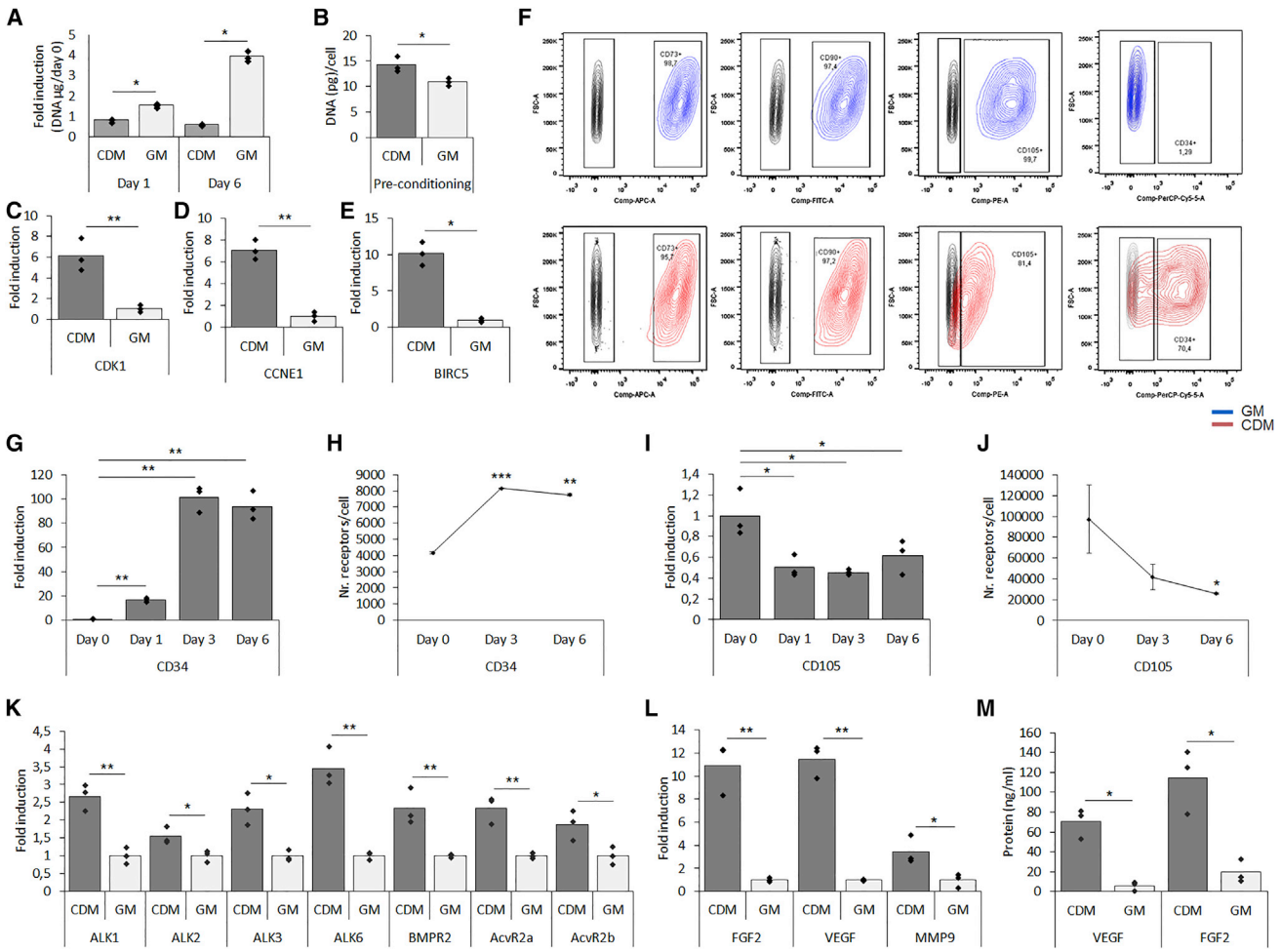

Figure 1. Serum-free Pre-conditioning for 6 Days Affected Cellular Identity

(A) DNA quantification in cells pre-conditioned in CDM or GM normalized to day 0.

(B–E) DNA per cell after 6 days of pre-conditioning (B). Pre-conditioning induced expression of cell cycle regulators *CDK1* (C), *CCNE1*(D), and *BIRC5* (E).

(F) Flow cytometry analysis after pre-conditioning for MSC markers CD73, CD90, and CD105 together with CD34.

(G and H) Kinetics studies on (G) the mRNA transcript level of *CD34* and (H) flow cytometry data on the number of CD34 molecules per cell.

(I and J) Kinetic studies on (I) the mRNA transcript level of *CD105* and (J) flow cytometry data on the number of CD105 molecules per cell.

(K–M) mRNA transcript analysis of BMP type 1 and type 2 receptors (K), *FGF2*, *VEGF*, and *MMP9* (L), confirmed on the protein level from conditioned medium (M).

n = 3, *p < 0.05, **p < 0.01, ***p < 0.001.

hPDCs were pre-conditioned in CDM or GM followed by 24 hr, or 3 or 6 days of BMP-2 stimulation in CDM. After 6 days, morphological differences between the two conditions were seen (Figure 2A). Cells pre-conditioned under serum-containing conditions displayed a heterogeneous cell population with a fraction possessing a polygonal shape resembling differentiating cells (black arrows). Interestingly, BMP-2-stimulated cells pre-conditioned in CDM displayed a more homogeneous cell morphology in which the majority of the cells exhibited a polygonal shape (black arrows). This phenomenon was associated with an increase in alkaline phosphatase (ALP) activity since a 3- and 1.5-fold increase was observed after 3 and 6 days of BMP stimulation, respectively (Figure 2B). To confirm the differentiation stage of the cells, mRNA transcripts were analyzed. After 24 hr of BMP-2 stimulation, a 2-fold upregulation of *SRY* (sex determining region *Y*)-*Box* 9 (*SOX9*) was seen in BMP-2 stimulated samples and this effect was further elevated to over 10-fold in day 3 and day 6 samples (Figure 2C). Moreover, CDM pre-conditioned cells displayed a 1.6- and 2-fold elevated expression compared with serum conditions in day 3 and 6 samples. Similarly, the osteogenic marker

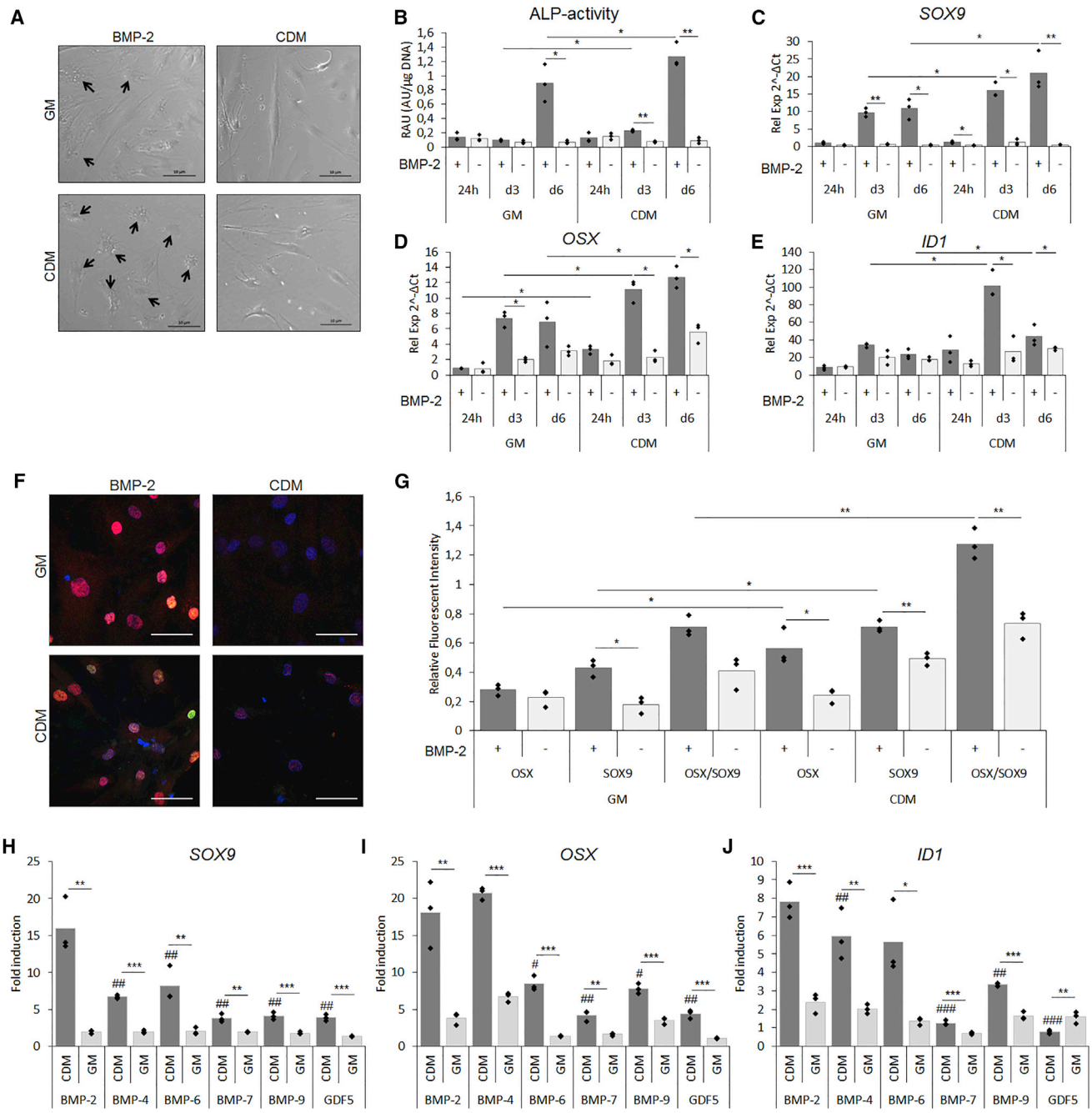

Figure 2. Serum-free Pre-conditioning led to Enhanced BMP-2-Induced Osteochondrogenic Differentiation In Vitro

After 6 days of pre-conditioning followed by 6 days of BMP-2 stimulation in CDM, a difference in response to BMP-2 was observed.

(A) Bright-field images after 6 days of BMP-2 stimulation indicating differentiated cells (black arrows).

(B–E) BMP-2 stimulation induced elevated ALP activity(B). mRNA transcripts displayed elevated expression of *SOX9* (C), *OSX* (D), and *ID1* (E) after 24 hr, and 3 and 6 days of BMP-2 stimulation.

(F) IHC for SOX9 (red) and OSX (green) with DAPI (blue) as nuclear stain after 6 days of BMP-2 stimulation.

(G–J) Quantification of merged confocal images expressed as relative units (RU) normalized to DAPI (G). mRNA transcript analysis after pre-conditioning of hPDCs followed by 6 days of stimulation of BMP-2, -6, -7, -9, and GDF5 depicted by *SOX9* (H), *OSX* (I), and *ID1* (J). Scale bar, 50 µm; n = 3, $^{*/\#}p < 0.05$, $^{**/\#\#}p < 0.01$, $^{***/\#\#\#}p < 0.001$ where $^{\#}$ represents statistical significance to BMP-2 treated condition.

Osterix (*OSX*) was upregulated in CDM pre-conditioned cells with a 1.6- and 1.9-fold increase after 3 and 6 days, respectively (Figure 2D). In support of the enhanced osteochondrogenic differentiation profiles of CDM pre-conditioned cells, analysis of collagen type 2a (*COLL2A1*), collagen type 10 (*COLL10A1*), runt-related transcription factor 2 (*RUNX2*), and collagen type 1 (*COLL1A1*) is presented in Figure S2A. Activated BMP signaling was confirmed by inhibitor of differentiation 1 (*ID1*) expression, a 2.5- and 2-fold higher expression was seen in CDM pre-conditioned cells after 3 and 6 days, respectively (Figure 2E).

Pre-conditioned Cells Undergo Osteochondrogenic Differentiation

The mRNA transcript analysis suggested a robust chondrogenic as well as osteogenic differentiation in cells pre-conditioned in CDM. To define whether there was a subpopulation of cells that differentiated toward a specific lineage, a combined immunohistochemistry (IHC) for SOX9 (red), OSX (green), and DAPI (blue) was performed. Cells displayed similar positivity for SOX9 in both BMP-2-stimulated conditions, but a larger fraction of OSX-positive cells in CDM pre-conditioned cells, mainly in combination with SOX9 positivity (Figure 2F). Quantification of merged images confirmed elevated positivity for both markers in CDM pre-conditioned cells followed by BMP-2 stimulation (Figure 2G). Of note, the enhanced BMP response in CDM pre-conditioned cells was not specific for BMP-2. In fact, this was consistent for a range of BMPs including BMP-4, -6, -7, -9, and GDF5. Upon mRNA transcript analysis of *SOX9* and *OSX*, a more than 2-fold increase was seen for all BMPs in cells pre-conditioned in CDM (Figures 2H and 2I). A similar phenomenon was seen for the BMP target gene *ID1* (Figure 2J). The elevated osteochondrogenic differentiation was further supported by analysis of aggrecan (*ACAN*), osteocalcin (*OCN*), distal-less homeobox 5 (*DLX5*), *BMP-2*, and *VEGF* (Figure S2B). The effect of CDM pre-conditioning was confirmed in young and adult donors, and presented in Supplemental Information (Figure S3A–S3G). Upon ectopic in vivo implantation for 3 weeks, CDM pre-conditioning followed by BMP-2 stimulation led to elevated cartilaginous matrix formation compared with GM-stimulated cells (Figure S4). These data show that serum-free pre-conditioning uniquely leads to an increased differentiation response to several BMP ligands. This effect is independent of donor gender or age and in vitro findings were translated in the in vivo setting.

Enhanced Differentiation due to an Altered BMP Pathway Activation

Western blot analysis of the pre-conditioned cells after 60 min of BMP-2 stimulation displayed an altered BMP signaling pathway activation compared with GM control (Figures 3A–3E). Quantification displayed elevated phosphorylation of the SMAD1/5/8 complex and p38 in the CDM pre-conditioned cells, while cells stimulated under GM conditions displayed phosphorylation of ERK1/2 and p38 (Figures 3F–3H). Since BMP signaling is known to crosstalk with downstream regulators of Wnt and transforming growth factor β, the activation of β-catenin and the SMAD2/3 complex was investigated. It was shown that BMP stimulation under GM conditions led to an increased level of active β-catenin, while CDM pre-conditioned cells displayed phosphorylation of the SMAD2/3 complex (Figures 3I and 3J). Together, these data confirm that the enhanced osteochondrogenic differentiation observed in the CDM pre-conditioned cells was associated with an altered downstream signaling activation.

The CD34$^+$ Cell Population Displayed a More Potent Osteochondrogenic Potential

To investigate whether it was the CD34$^+$ cell population that was more BMP responsive, pre-conditioned CD34$^+$ cells were sorted and compared with the total CDM population. On the mRNA transcript level, elevated CD34 expression was confirmed (Figure 3K). Interestingly, an upregulated expression of BMP receptors *ALK1* and *ALK6* was confirmed, whereas an upregulated trend was detected for *ALK2* and *BMPR2*, and no difference was found for *ALK3* (Figure 3L). Upon BMP-2 stimulation, the CD34$^+$ population displayed a 2- and 5-fold elevated expression of *SOX9* and *OSX*, respectively (Figure 3M). Cluster analysis displayed a correlation between elevated *CD34*, *ALK1*, *ALK2*, *ALK6*, *BMRP2*, *SOX9*, and *OSX* expression (Figure 3N), and specific grouping of the CD34$^+$ population was depicted in a constellation plot (Figure 3O). Combined, these data indicate that the increased osteochondrogenic response is related to the CD34$^+$ cell population.

Bioinspired 3D Aggregation and BMP-2 Stimulation Reduce Stemness and Cell Size

Cellular condensations precede limb bud development and therefore aggregation was investigated in order to enhance cell specification in hPDCs by providing biomimetic 3D cues. Aggregate size affects mechanical cues, nutrient flux, and cell-cell interaction forces. Optimal aggregate size was determined through an in vitro screening of 50, 100, and 250 hPDCs/aggregate. Cell aggregation was induced on pre-conditioned cells with or without BMP-2 stimulation for 6 days, after which the samples were analyzed by microscopy, mRNA transcript analysis, histology, and IHC. 2D-cultured cells were included as a control. Bright-field images showed that uniform aggregates were formed in the 100 and 250 cell aggregate size (Figure S5A). Next, the influence of

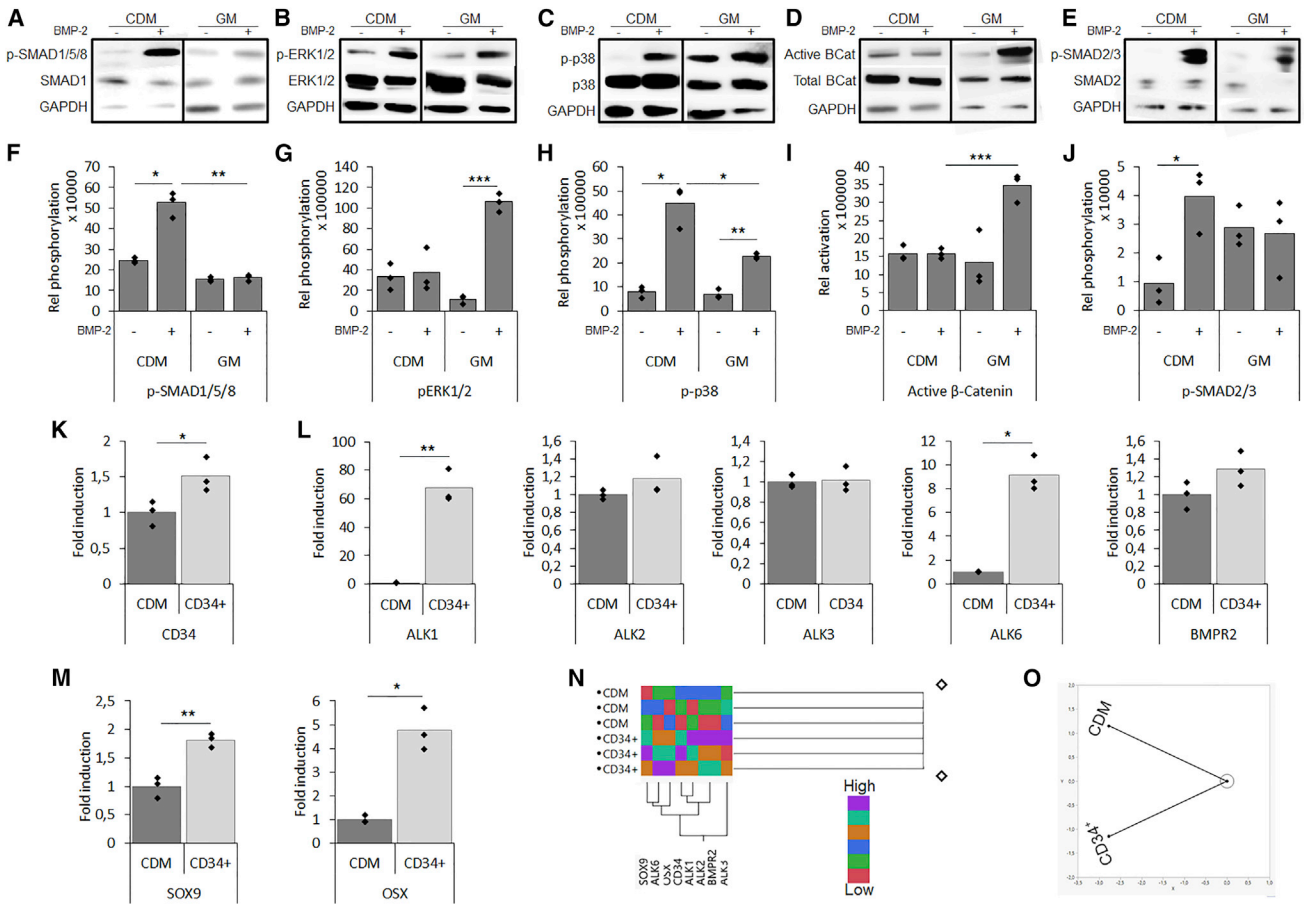

Figure 3. Altered Pathway Activation upon Pre-conditioning with CD34$^+$ Cells Displaying a More Potent Osteochondro-Progenitor Cell Population

(A–J) Pathway activation following pre-conditioning and BMP-2 stimulation investigated by western blot and subsequent quantification for (A) and (F) p-SMAD1/5/8, (B) and (G) p-Erk1/2, (C) and (H) p-p38, (D) and (I) active β-catenin, and (E) and (J) p-SMAD2/3.
(K and L) Following separation of the CD34$^+$ cell population, elevated expression of CD34 (K) and BMP receptors (L) were seen.
(M) Following 6 days of BMP-2 stimulation the CD34$^+$ hPDCs showed elevated differentiation depicted by *SOX9* and *OSX* expression.
(N) Cluster analysis displayed a correlation between the expression of CD34, BMP receptors, and differentiation markers.
(O) A constellation plot showed clear grouping of CD34$^+$ cells and the total cell population.
n = 3, *p < 0.05, **p < 0.01, ***p < 0.001.

aggregation and BMP-2 stimulation on the MSC markers CD73, CD90, and CD105 was investigated by flow cytometry (Figure 4A). The analysis of CD73 showed a reduced positivity from 96% to below 80% in aggregated cells in the presence of BMP-2. This effect was even more pronounced for CD90 with less than 45% positivity. The largest reduction was seen when analyzing CD105 expression: only 19% of the cells cultured in an aggregate system and stimulated with BMP-2 were positive compared with 96% in only aggregated cells. Moreover, aggregation induced a reduction in cell size compared with both the control and BMP-2-stimulated cells in 2D (Figure S5B). These data indicate that an aggregation-dependent effect on the CD34-enriched hPDC population was induced, further enhanced in combination with BMP-2 stimulation.

Aggregation and BMP-2 Treatment Synergistically Enhance In Vitro Osteochondrogenic Differentiation

Upon mRNA transcript analysis, BMP-2 stimulation induced an elevated expression of the chondrogenic markers *SOX9*, *COLL2A1*, and *ACAN* (Figure 4B), and the largest increase in expression was found in cells stimulated in 2D. Upon analysis of osteogenic markers *RUNX2*, *ALP*, and *OSX*, a synergistic effect of aggregation in combination with BMP-2 stimulation was seen, which was further increased with aggregate size (Figure 4C). The upregulated differentiation profile could be correlated to the expression

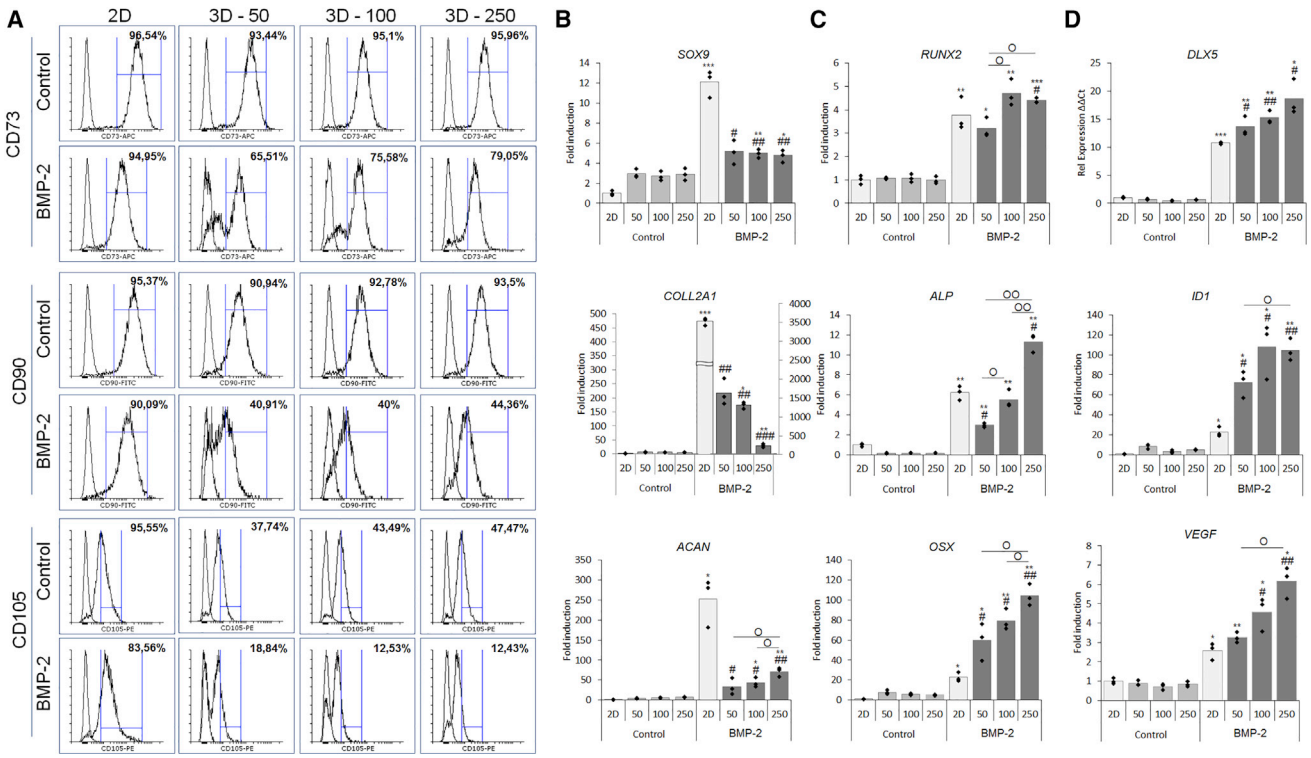

Figure 4. The Number of Cells per Aggregate Affected Osteogenic and Chondrogenic Cell Specification

To determine optimal size, aggregates of 50, 100, and 250 cells/aggregate were investigated after 6 days of aggregation.

(A–D) Aggregation and BMP-2 stimulation induced a shift in MSC marker expression and a reduction when both factors were combined (A). mRNA transcript analysis of (B) chondrogenic, (C) osteogenic, and (D) BMP signaling and angiogenic markers indicated that both aggregation, aggregation size and BMP-2 stimulation affected cell differentiation. n = 3, statistical significance to non-BMP-2-stimulated conditions: *$p < 0.05$, **$p < 0.01$, ***$p < 0.001$ and to 2D BMP-2 conditions: $^{\#}p < 0.05$, $^{\#\#}p < 0.01$, $^{\#\#\#}p < 0.001$.

of the transcriptional regulator *DLX5*, the BMP marker gene *ID1*, and the angiogenic marker *VEGF* (Figure 4D). Next, the gene expression data were confirmed on the protein level by IHC for SOX9 (red), OSX (green), and DAPI (blue) (Figure S6A). Histology for H&E, Alcian blue (AB) and alizarin red displayed the initiation of matrix formation in the in vitro stimulated microtissues, depicted in stained sections of 250 hPDCs/aggregate (Figure S6B). These data confirmed the induction of osteochondrogenic cell specification induced by the 3D environment, in which the aggregate size steered differentiation in combination with BMP-2.

In Vivo Ectopic Tissue Formation

Based on the in vitro analysis, the size of 250 cells/aggregate was selected for in vivo evaluation combined with or without simultaneous BMP-2 stimulation in parallel to 2D-stimulated cultures. In addition, 2D cultures stimulated with BMP-2 for 6 days followed by 24 hr of aggregation in the absence of BMP-2 were included in order to evaluate the combined as well as the individual effects of aggregation and BMP stimulation. Upon analysis of implants harvested after 1 week, H&E staining displayed microvessel formation (black arrows) which was shown to be 2-fold higher in samples treated with BMP-2. This effect was synergistic when combined with aggregation (Figures 5A and 5E). An AB staining revealed the deposition of cartilaginous matrix, rich in GAG content, in BMP-2-treated aggregates (black arrows) (Figure 5B), confirmed by Masson's trichrome (MT) stain, which displayed a more mature matrix tissue with a denser collagen content (black arrows) (Figure 5C). IHC for p-SMAD1/5/8 showed active BMP signaling in explants that were cultivated in the presence of BMP-2 or aggregated, depicted by brown nuclei (black arrows) (Figure 5D). When combined, the number of positive nuclei was further increased (black arrows). These data were confirmed by quantification of positive nuclei normalized to the total number of nuclei (Figure 5F). Due to the active BMP signaling, analysis of endogenous BMP-2 production was investigated by ELISA in conditioned medium at the time of implantation (Figure 5G). The combined effect of BMP-2 stimulation and aggregation displayed 1.5-fold higher BMP-2 protein levels in conditioned medium compared with fresh stimulation medium. This

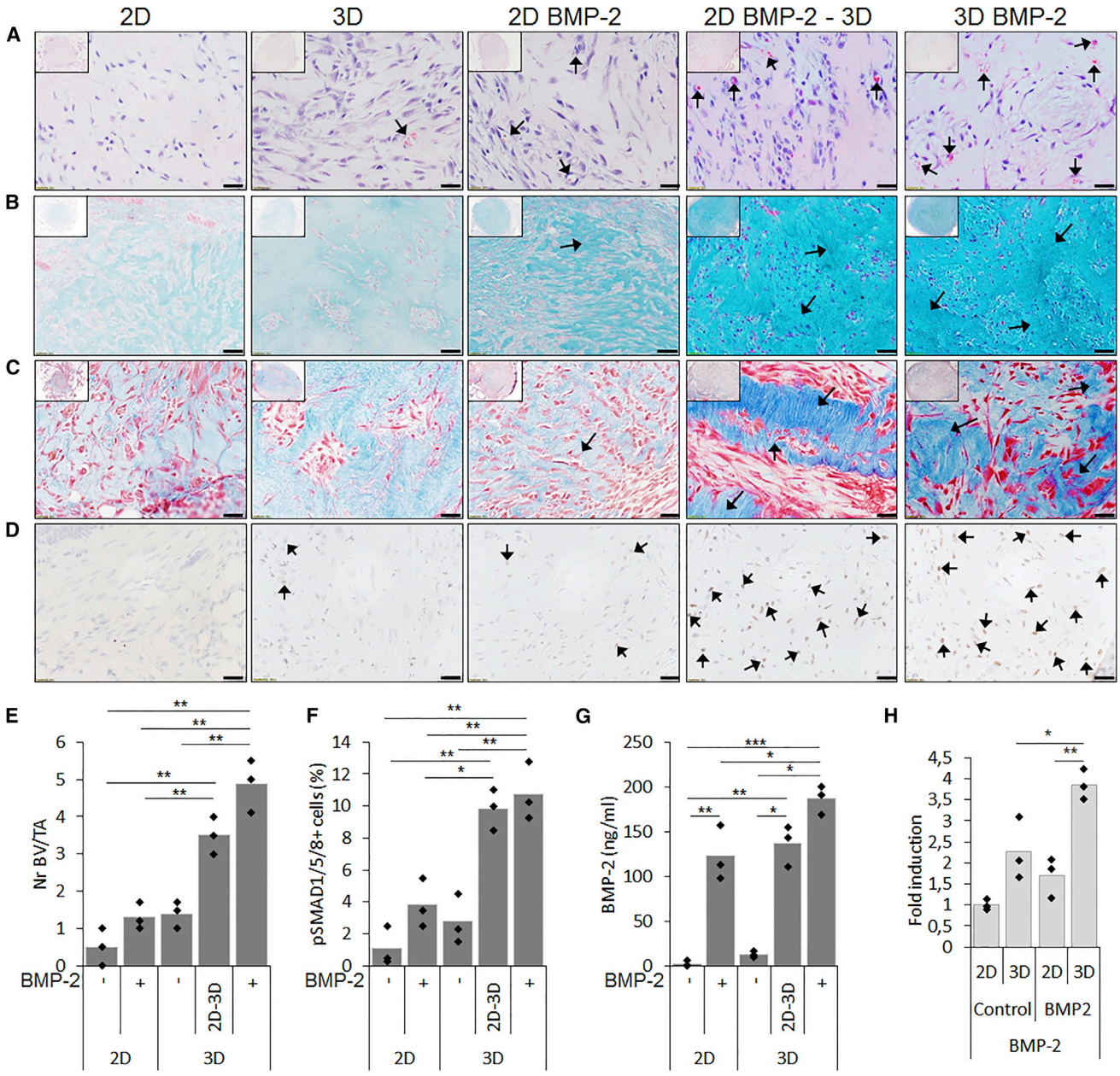

Figure 5. In Vitro Priming Leads to an In Vivo Cartilage Intermediate 1 Week Post Transplantation

Histology of tissue constructs 1 week after in vivo subcutaneous implantation displayed that both BMP-2 stimulation and aggregation affected in vivo tissue formation.

(A) H&E staining showed microvessel formation (black arrows).

(B and C) Denser AB staining revealed more cartilage matrix accumulation (black arrows) (B), confirmed by denser collagen staining by MT staining (black arrows) (C).

(D) Upon IHC for p-SMAD1/5/8 as a marker for active BMP signaling, positive nuclei (brown stain, black arrows) were seen in samples stimulated by BMP-2 and/or aggregation.

(E and F) Quantification showed that the combined stimulation of BMP-2 and aggregation elevated the number of microvessels (E) and positive nuclei for p-SMAD1/5/8 (F).

(G) BMP-2 production by stimulated cells were confirmed in conditioned medium by ELISA.

(H) Enhanced transcripts for *BMP-2* on implants at the time of implantation.

Scale bars, 20 μm. n = 4, *p < 0.05, **p < 0.01, ***p < 0.001.

finding was further confirmed by enhanced mRNA transcript levels of BMP-2 expression at the time of implantation (Figure 5H).

After 3 weeks, H&E staining displayed the presence of hypertrophic chondrocytes in BMP-2-stimulated aggregates (3D) (black arrows), a phenomenon that was not seen in 2D stimulated cells followed by aggregation (2D-3D) (Figure 6A). An AB stain confirmed the formation of a dense matrix rich in GAGs (white arrows) (Figure 6B). These findings were further supported by an MT staining (Figure 6C). To analyze remodeling of the cartilaginous matrix, tartrate-resistant acid phosphatase (TRAP) staining was performed, which showed positive areas in close vicinity to GAG-rich areas and hypertrophic chondrocytes (black arrows) (Figure 6D). Upon quantification, the BMP-2-stimulated aggregates displayed a 2-fold higher percentage of $TRAP^+$ area (Figure 6E). Remodeling of the cartilage intermediate was further confirmed by IHC for DIPEN, the cryptic epitope of ACAN, typically exposed upon its degradation (black arrows) (Figure 6F). To further characterize the cartilaginous tissue, IHC for S100 confirmed a 6-fold higher positive area in BMP-2-stimulated aggregates (black arrows) (Figures 6G and 6H). Furthermore, a mature cartilaginous tissue was confirmed by IHC for Indian hedgehog (Ihh), expressed by (pre)hypertrophic chondrocytes (black arrows) (Figures 6I and 6J).

After 6 weeks, the 3D stimulated tissue intermediate had further developed along the endochondral route to form ectopic mineralized tissue (Figure 6K). Formation of bone ossicles were confirmed through H&E and MT staining. Bone (black arrows) and bone marrow (red arrows) were observed as well as zones of mature bone (green arrows) (Figure 6L). Active remodeling (blue arrows) was indicated by a TRAP staining while contribution of the implanted cells was confirmed by IHC specific for human osteocalcin (hOCN). These data confirm the in vivo maturation and reveal that the combined approach of cell aggregation and exposure to BMP-2 induced in vivo tissue development in a process closely resembling endochondral bone formation.

Healing of a Critical Size Long-Bone Defect

Based on the ectopic endochondral development of the in vitro primed microtissues, the orthotopic behavior was next assessed in a critical size tibia defect in immunodeficient mice. Upon transplantation, the in vitro BMP-2-stimulated aggregates led to bridging within 4 weeks as assessed by X-ray analysis in five of six animals (Figure 7A). Non-unions were confirmed in four of five controls up to 8 weeks after the creation of the defects. Full bridging by a mineralized matrix at 4 and 8 weeks was confirmed by nano-computed tomography scanned explants (Figure 7B). Qualitative analysis was assessed by histology and IHC. H&E and Safranin O/fast green staining revealed a cartilage intermediate 2 weeks post implantation (Figures 7C and 7D). Hypertrophic chondrocytes were present (gray arrows) in the center of the cartilaginous callus, whereas a mineralized tissue had started to form in the periphery, the latter being visualized by MT staining (black arrows) (Figure 7E). The early cartilage intermediate displayed positivity for TRAP (blue arrows), suggesting remodeling of the mineralized cartilaginous intermediate, a process that was maintained at week 4 but decreased at week 8 (Figure 7F). Moreover, the cartilage callus displayed positivity for hOCN, depicted by a brown stain (white arrows), confirming the contribution of donor cells (Figure 7G). At 4 weeks, a fully mineralized bridging was observed, where the MT staining showed more mature mineralized zones, indicated by red zones (yellow arrows) (Figure 7E). This mineralized tissue stained positive for hOCN (white arrows) (Figure 7G). After 8 weeks, the mineralized matrix displayed more zones of mature bone which was also confirmed to be positive for hOCN (white arrows) (Figures 7F and 7G). In addition, qualitative analysis confirmed the absence of cartilage or osseous tissue in control non-unions as well as a negative staining for hOCN (Figures 7C–7G). These data demonstrate a successful bridging of a critical size fracture by an in vitro primed cell-based construct.

DISCUSSION

Cell-based ATMPs represent an opportunity for the qualitative long-term cure of incapacitated organs or tissues lacking adequate intrinsic biological potential to heal (Einhorn and Gerstenfeld, 2015). Despite scientific breakthroughs, only a fraction of the developed ATMPs today reaches success in clinical translation for many reasons, including the poor design of the ATMP, modest outcomes in rigorous clinical trials, manufacturing challenges, and cost of goods (Erben et al., 2014). To drive successful clinical translation, a deeper understanding of the basic biology that underlies (1) the mechanism of the healthy repair process that is failing and (2) the design of the engineered construct, is required (Loh et al., 2016). As a driving force in developing a clinically effective ATMP for large long-bone defect healing, the choice of progenitor cells is of importance where the periosteum represents a relevant tissue source. Autologous hPDCs can be isolated at the site of the fracture without a second surgery. However, there are limitations in terms of the amount of tissue available. The use of allogenic cells may allow harvest of larger tissues depending on the donor, but comprises the risk of disease transmission and immune response (Morizane et al., 2013). Consequently, current cell culture protocols focus on achieving

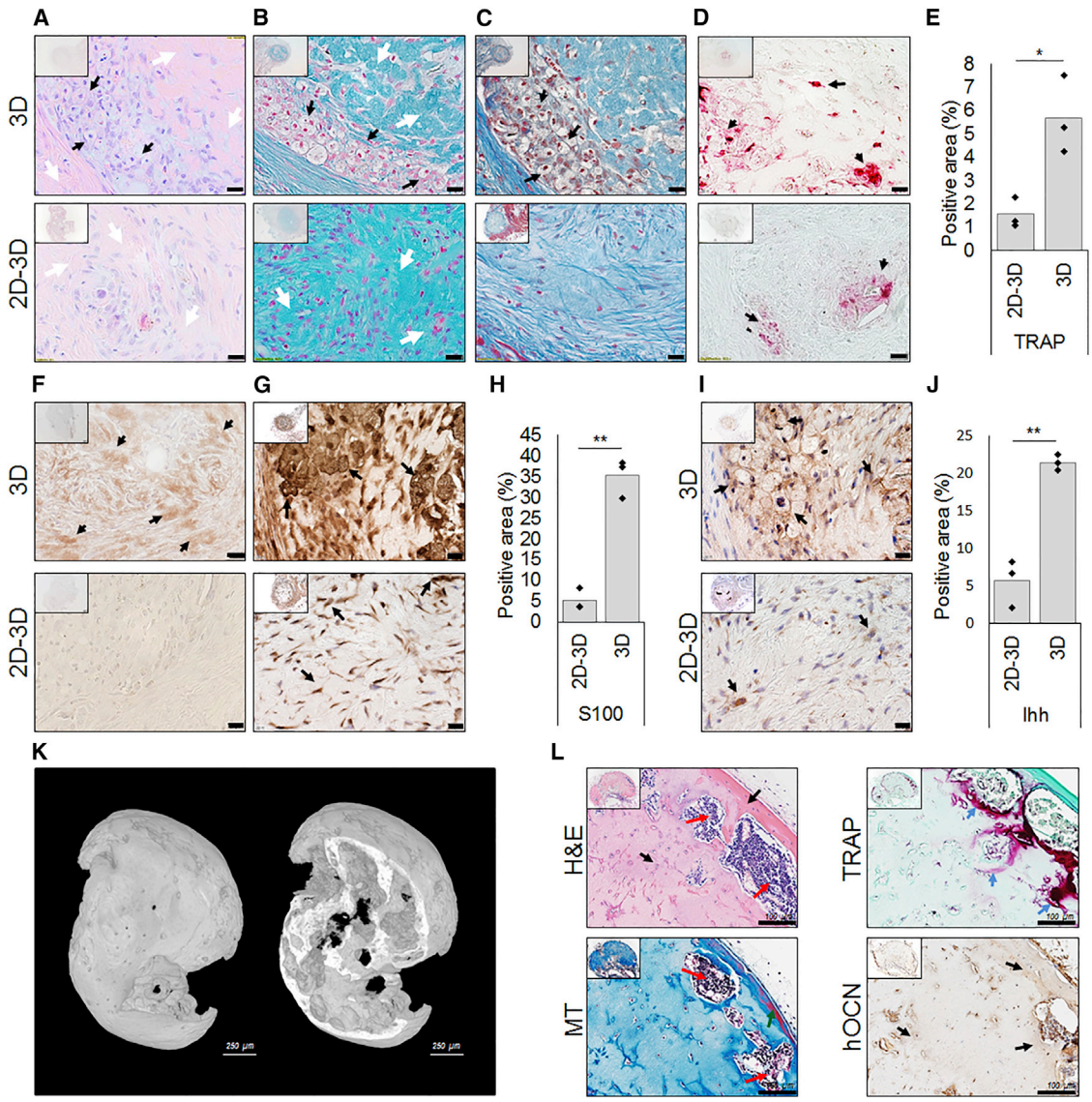

Figure 6. The Combined In Vitro Priming by BMP-2 Treatment and Aggregation Led to Endochondral Bone Formation In Vivo

Histology on tissue constructs 3 weeks after in vivo subcutaneous implantation demonstrated that the simultaneous stimulation by aggregation and BMP-2 affected in vivo tissue formation.

(A) H&E staining displayed the presence hypertrophic chondrocytes (black arrows) next to denser ECM areas (white arrows).

(B) Denser AB stain lines the zones of hypertrophic chondrocytes (white arrows) surrounded by GAG-rich areas (white arrows).

(C) The MT stain confirmed the formation of denser areas (black arrows).

(D and E) TRAP-positive areas (black arrows) surrounding the hypertrophic chondrocytes suggest remodeling (D) and quantification (E).

(F) IHC for DIPEN showed breakdown of GAG-rich areas.

(G and H) IHC for S100 displayed more mature cartilage tissue in BMP-2 stimulated aggregates (G), confirmed by quantification (H).

(I and J) IHC for Ihh showed the presence of hypertrophic chondrocytes (I), which upon quantification was a 4-fold higher compared with 2D-stimulated cells (J).

(K) At 6 weeks, the endochondral tissue intermediate had developed into a mineralized ossicle.

(L) H&E staining confirmed de novo formed bone (black arrows) and bone marrow (red arrows), while MT staining displayed zones of mature bone (green arrows). TRAP staining suggested ongoing remodeling of immature bone (blue arrows) and IHC for hOCN confirmed the contribution of the implanted cells. Unlabeled scale bars, 20 µm. n = 4, *p < 0.05, **p < 0.01.

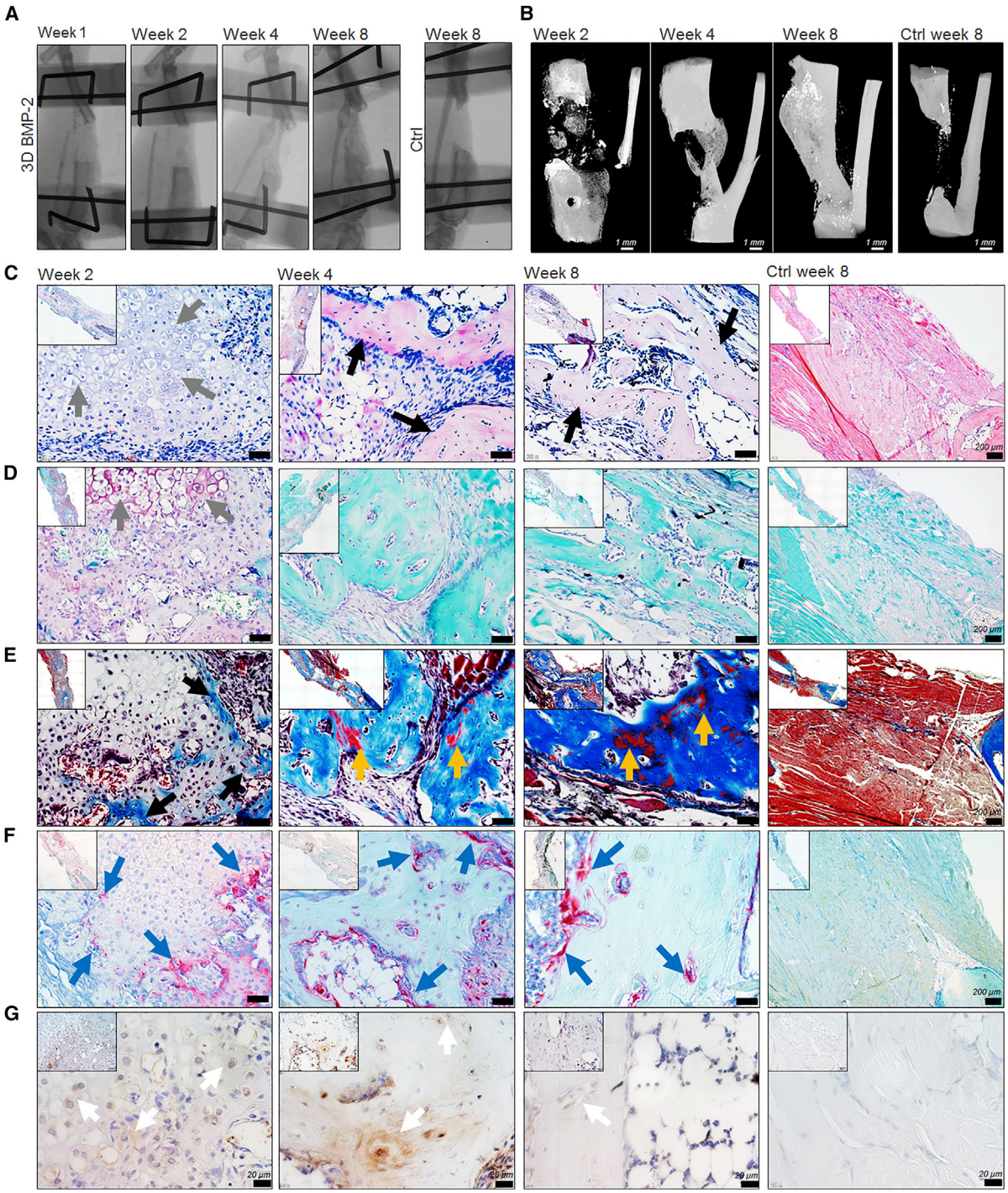

Figure 7. The In Vitro Primed Cell-based Tissue Construct Led to the Healing of a Critical Size Long-Bone Defect

(A) In vivo X-ray monitoring of fracture healing upon transplantation of in vitro BMP-2-stimulated microaggregates.

(B) Reconstructed images from nano-computed tomography scanned explants displayed mineralized healing of the critical-sized defect 4 weeks post transplantation.

(C–G) Qualitative analysis of sectioned explants 2, 4, and 8 weeks post transplantation, including control confirming non-union. Cartilage and bone formation was confirmed by H&E (C), Safranin O and fast green (D), and MT (E) staining. Tissue remodeling was investigated by a TRAP stain (F), whereas contribution of implanted cells was confirmed by IHC for hOCN (G). Arrows indicate specific tissues as follows: cartilage (gray), bone (black), mature bone (yellow), TRAP-positive areas (blue), hOCN-positive cells, and matrix (white). Unlabeled scale bar, 50 µm.

a fast and efficient expansion phase without an appreciation of maintenance of the progenitor potential.

In addition, recent findings indicate that the majority of in vitro expanded cells undergo apoptosis upon implantation (Stegen et al., 2016). A cause may be the need to instantly adjust to a compromised environment, since current culture conditions represent a rather non-physiological and abundant nutritional source. Optimized culture conditions for clinically relevant progenitors are therefore essential for the in vitro preparation of cell-based constructs and should maintain cell survival, allow efficient growth factor treatments without batch-to-batch variation, and meet the regulatory guidelines (Dimarakis and Levicar, 2006).

We developed a serum-free pre-conditioning regime in a CDM in order to adapt/prepare progenitor cells for differentiation and the subsequent in vivo environment. Of note, pre-conditioning in CDM led to an increased DNA content per cell, but no cell proliferation or change in karyotype profile. This suggests the onset of endoreplication, a phenomenon where cells replicate the nuclear genome in the absence of cell division, leading to elevated DNA content and enhanced cell potential in order to save energy (Edgar and Orr-Weaver, 2001). This was further supported by increased mRNA transcript levels of the cell cycle markers *CCNE1*, *CDK1*, and *BIRC5* (Banyai et al., 2016; Britton and Edgar, 1998; Yamamoto et al., 2008). Although the mechanism of endoreplication is not yet fully understood, studies in mice have shown improved adaptation to stress and/or limited energy sources, typically seen during tissue regeneration (Pandit et al., 2013; Sher et al., 2013). Although more studies are needed in order to elucidate whether cells from the periosteum adapt this mechanism after the initial proliferative burst in fracture healing, this may be a potential cause of their remarkable regenerative capacity (Roberts et al., 2015), a phenomenon partially replicated by the pre-conditioning.

Furthermore, a dramatic shift in MSC marker expression was seen, including an increased positivity for CD34 (Wood et al., 1997; Fina et al., 1990; Krause et al., 1994). There is evidence that CD34 is a marker for diverse progenitors including MSCs (Copland et al., 2008). In the current study, mRNA transcript levels of *CD34* were higher in freshly isolated hPDCs grown to confluency. This indicates that native progenitors from the periosteum may be $CD34^+$, but the expression is lost upon in vitro expansion. This is in line with previous reports with murine bone marrow mononuclear progenitors, defined as a potent osteoprogenitor cell population, losing their $CD34^+$ upon in vitro expansion (Abdallah et al., 2015). Moreover, the $CD34^+$ cell population displayed an enhanced expression and secretion of osteoprogenitor-secreted factors (Majka et al., 2001; Janowska-Wieczorek et al., 2002). In addition, an elevated expression of BMP type 1 and 2 receptors was seen, suggesting the generation of a more BMP-responsive cell population (Hidalgo et al., 2012). In line with these findings, CDM pre-conditioned hPDCs displayed an earlier onset of, as well as an elevated osteochondrogenic response to BMP treatment, confirmed by BMP-2, -4, -6, -7, -9, and GDF5 stimulation. This improved differentiation potential could be correlated to the $CD34^+$ cell population. In addition, an altered activation of downstream signaling pathways was confirmed in the CDM pre-conditioned cells, suggesting a potential mechanism to the more potent differentiation. Importantly, a change in cellular phenotype and improved differentiation potential was observed in cells isolated from donors of different gender and age, in line with previous reports on the osteochondrogenic capacity of PDCs (Chang et al., 2014). Of note, a reduced response was seen in cells isolated from a 47-year-old female, which was associated with low expression levels of BMP receptors. Further screening of more samples will be required to determine whether this is a combined age- and gender-dependent phenomenon (Nicks et al., 2010). Since both an elevated osteogenic as well as chondrogenic differentiation was seen, IHC for SOX9 and OSX was performed to gain information at the single-cell level. Remarkably, CDM pre-conditioned cells displayed a positivity for both markers. Cell-fate studies have revealed that SOX9-expressing limb bud mesenchymal cells give rise to both chondrocytes and osteoblasts, where SOX9 expression precedes RUNX2 and OSX expression during limb bud development (Akiyama et al., 2005; Nakashima et al., 2002). As a consequence, the combined SOX9 and OSX positivity may reflect the stage when cells enter the hypertrophic or early osteoblast stage and undergo a transition from $SOX9^+$ to OSX^+ cells. On the other hand, additional markers such as *ACAN*, *COLL10A1*, *RUNX2*, and *OCN* are also upregulated, further opening the possibility of cells undergoing a dual- or trans-differentiating pathway (Yang et al., 2014; Zhou et al., 2014). Nevertheless, the elevated differentiation capacity seen in vitro could be correlated to an elevated cartilaginous tissue production in vivo. To further investigate the in vivo potential, a biomimetic system in the form of cell aggregation was introduced (Moreira Teixeira et al., 2012; Evans et al., 2013). Initially, an optimal size of the aggregate was determined and an increased aggregate size led to elevated expression of *RUNX2*, *ALP*, *OSX*, and *VEGF*. This could potentially be explained by the elevated forces exerted by the increased number of cells in the aggregates, which further steered differentiation toward the endochondral fate (Qi et al., 2008; Mammoto et al., 2011). Upon ectopic assessment in vivo, a synergistic effect of aggregation and BMP-2 treatment displayed an enhanced microvessel ingrowth along with the presence of GAG-rich matrix and active BMP signaling. It can be

speculated that this was due to endogenous BMP production suggested by an elevated BMP-2 protein secretion, further supported by elevated *BMP-2* expression on an mRNA transcript level. Therefore, the endogenous BMP secretion may further have contributed to in vivo endochondral bone formation (Einhorn, 1998; Schindeler et al., 2008). After 3 weeks in vivo, the presence of hypertrophic chondrocytes, cartilage remodeling, and degradation was observed in constructs where simultaneous stimulation by aggregation and BMP-2 was applied. At week 6, these constructs had further developed into bone ossicles. Assessment in a critical size long-bone defect displayed successful bone bridging 4 weeks post transplantation. Qualitative analysis at 2 weeks displayed a process resembling endochondral bone healing with the contribution of the transplanted hPDCs to both the intermediate cartilage tissue as well as the bridging bone. A reduced contribution of the implanted cells was seen at week 8, suggesting that host-derived cells are involved in the remodeling of the newly formed bone tissue.

This study reports the development of a cell-based strategy for the healing of a critical size long-bone defect through a cartilaginous intermediate using a serum-free, chemically defined, and biomimetic approach. In vitro BMP-2 treatment of cell-based bioinspired engineered microtissues leads to a primed but not mature cartilage tissue, self-sustained by endogenous production of growth and differentiation factors. Upon in vivo implantation, tissue formation is achieved in a process mimicking natural fracture healing. Encouragingly, this approach is applicable for autologous as well as allogenic progenitor cell populations. The presented findings represent a fundamental contribution to the successful development of clinically relevant cell-based constructs for tissue regeneration and provide convincing information on the importance of relevant in vitro conditions for the in vivo outcome.

EXPERIMENTAL PROCEDURES

Pre-conditioning in CDM or GM as a control was carried out for 6 days. Directly following pre-conditioning, BMP-2 stimulation and/or aggregation was carried out for an additional 6 days. In vivo implantation was carried out ectopically and orthotopically in NMRI$^{nu/nu}$ mice. Cell material was encapsulated in collagen type 1 gels for implantation. In vivo development of the implanted constructs was studied for up to 8 weeks. Detailed experimental procedures are provided in the Supplemental Information. The ethical committee for human medical research (KU Leuven) approved all procedures, and informed consent was obtained from the patients. All procedures on animal experiments were approved by the local ethical committee for animal research (KU Leuven). The animals were housed according to the guidelines of the Animalium Leuven (KU Leuven).

SUPPLEMENTAL INFORMATION

Supplemental Information includes Supplemental Results, Supplemental Experimental Procedures, six figures, and one table and can be found with this article online at http://dx.doi.org/10.1016/j.stemcr.2017.01.005.

AUTHOR CONTRIBUTIONS

The contribution of each author is as follows; J.B., planning, experimental design, experimental work, data collection and analysis, and manuscript drafting. W.J., experimental design and experimental work. J.L., L.M.T., D.L., and M.C., experimental work. V.B., experimental design. F.P.L., experimental design and data interpretation. All authors have read and accepted the final manuscript.

ACKNOWLEDGMENTS

This work is part of Prometheus, the KU Leuven R&D division for skeletal tissue engineering. http://www.kuleuven.be/prometheus. The authors would like to thank M. V.d. Broeck, K. Bosmans, L. Ceysens, S. Bellinkx, and W.L. Tam for excellent technical assistance. The research leading to these results has been funded by: IWT-SBO-111545, FP/2007–2013/ERC grant agreement nos. 249191, FWO (12S6817N, 12O8715N, 12C8214N, 12I6216N, and 12G2715N), KU Leuven (PDMK/14/203), and NWO (14328). Nano-computed tomography images were generated in the X-ray computed tomography facilities of the Department of Materials Engineering of the KU Leuven, financed by the Hercules Foundation (project AKUL 09/001: Micro- and nano-CT for the hierarchical analysis of materials).

Received: June 11, 2016
Revised: January 6, 2017
Accepted: January 6, 2017
Published: February 9, 2017

REFERENCES

Abdallah, B.M., Al-Shammary, A., Skagen, P., Abu Dawud, R., Adjaye, J., Aldahmash, A., and Kassem, M. (2015). CD34 defines an osteoprogenitor cell population in mouse bone marrow stromal cells. Stem Cell Res. *15*, 449–458.

Akiyama, H., Kim, J.E., Nakashima, K., Balmes, G., Iwai, N., Deng, J.M., Zhang, Z., Martin, J.F., Behringer, R.R., Nakamura, T., and de Crombrugghe, B. (2005). Osteo-chondroprogenitor cells are derived from Sox9 expressing precursors. Proc. Natl. Acad. Sci. USA *102*, 14665–14670.

Baker, M. (2016). Reproducibility: respect your cells! Nature *537*, 433–435.

Banyai, G., Baidi, F., Coudreuse, D., and Szilagyi, Z. (2016). Cdk1 activity acts as a quantitative platform for coordinating cell cycle progression with periodic transcription. Nat. Commun. *7*, 11161.

Bolander, J., Ji, W., Geris, L., Bloemen, V., Chai, Y.C., Schrooten, J., and Luyten, F.P. (2016). The combined mechanism of bone morphogenetic protein- and calcium phosphate-induced skeletal

tissue formation by human periosteum derived cells. Eur. Cell Mater. *30*, 11–25.

Britton, J.S., and Edgar, B.A. (1998). Environmental control of the cell cycle in Drosophila: nutrition activates mitotic and endoreplicative cells by distinct mechanisms. Development *125*, 2149–2158.

Chang, H., Docheva, D., Knothe, U.R., and Knothe Tate, M.L. (2014). Arthritic periosteal tissue from joint replacement surgery: a novel, autologous source of stem cells. Stem Cells Transl. Med. *3*, 308–317.

Chappuis, V., Gamer, L., Cox, K., Lowery, J.W., Bosshardt, D.D., and Rosen, V. (2012). Periosteal BMP2 activity drives bone graft healing. Bone *51*, 800–809.

Colnot, C. (2009). Skeletal cell fate decisions within periosteum and bone marrow during bone regeneration. J. Bone Miner. Res. *24*, 274–282.

Colnot, C., Zhang, X., and Knothe Tate, M.L. (2012). Current insights on the regenerative potential of the periosteum: molecular, cellular, and endogenous engineering approaches. J. Orthop. Res. *30*, 1869–1878.

Copland, I., Sharma, K., Lejeune, L., Eliopoulos, N., Stewart, D., Liu, P., Lachapelle, K., and Galipeau, J. (2008). CD34 expression on murine marrow-derived mesenchymal stromal cells: impact on neovascularization. Exp. Hematol. *36*, 93–103.

De Bari, C., Dell'accio, F., Vanlauwe, J., Eyckmans, J., Khan, I.M., Archer, C.W., Jones, E.A., Mcgonagle, D., Mitsiadis, T.A., Pitzalis, C., and Luyten, F.P. (2006). Mesenchymal multipotency of adult human periosteal cells demonstrated by single-cell lineage analysis. Arthritis Rheum. *54*, 1209–1221.

Dimarakis, I., and Levicar, N. (2006). Cell culture medium composition and translational adult bone marrow-derived stem cell research. Stem Cells *24*, 1407–1408.

Edgar, B.A., and Orr-Weaver, T.L. (2001). Endoreplication cell cycles: more for less. Cell *105*, 297–306.

Einhorn, T.A. (1998). The cell and molecular biology of fracture healing. Clin. Orthop. Relat. Res., S7–S21.

Einhorn, T.A., and Gerstenfeld, L.C. (2015). Fracture healing: mechanisms and interventions. Nat. Rev. Rheumatol. *11*, 45–54.

Erben, R.G., Silva-Lima, B., Reischl, I., Steinhoff, G., Tiedemann, G., Dalemans, W., Vos, A., Janssen, R.T., Le Blanc, K., van Osch, G.J., and Luyten, F.P. (2014). White paper on how to go forward with cell-based advanced therapies in Europe. Tissue Eng. Part A. *20*, 2549–2554.

Evans, S.F., Docheva, D., Bernecker, A., Colnot, C., Richter, R.P., and Knothe Tate, M.L. (2013). Solid-supported lipid bilayers to drive stem cell fate and tissue architecture using periosteum derived progenitor cells. Biomaterials *34*, 1878–1887.

Eyckmans, J., Roberts, S.J., Bolander, J., Schrooten, J., Chen, C.S., and Luyten, F.P. (2013). Mapping calcium phosphate activated gene networks as a strategy for targeted osteoinduction of human progenitors. Biomaterials *34*, 4612–4621.

Fina, L., Molgaard, H.V., Robertson, D., Bradley, N.J., Monaghan, P., Delia, D., Sutherland, D.R., Baker, M.A., and Greaves, M.F. (1990). Expression of the CD34 gene in vascular endothelial cells. Blood *75*, 2417–2426.

Hidalgo, L., Martinez, V.G., Valencia, J., Hernandez-Lopez, C., Vazquez, M.N., Nunez, J.R., Zapata, A.G., Sacedon, R., Varas, A., and Vicente, A. (2012). Expression of BMPRIA on human thymic NK cell precursors: role of BMP signaling in intrathymic NK cell development. Blood *119*, 1861–1871.

Ingber, D.E., Mow, V.C., Butler, D., Niklason, L., Huard, J., Mao, J., Yannas, I., Kaplan, D., and Vunjak-Novakovic, G. (2006). Tissue engineering and developmental biology: going biomimetic. Tissue Eng. *12*, 3265–3283.

Janowska-Wieczorek, A., Majka, M., Marquez-Curtis, L., Wertheim, J.A., Turner, A.R., and Ratajczak, M.Z. (2002). Bcr-abl-positive cells secrete angiogenic factors including matrix metalloproteinases and stimulate angiogenesis in vivo in Matrigel implants. Leukemia *16*, 1160–1166.

Jung, S., Panchalingam, K.M., Rosenberg, L., and Behie, L.A. (2012). Ex vivo expansion of human mesenchymal stem cells in defined serum-free media. Stem Cells Int. *2012*, 123030.

Knothe Tate, M.L., Falls, T.D., Mcbride, S.H., Atit, R., and Knothe, U.R. (2008). Mechanical modulation of osteochondroprogenitor cell fate. Int. J. Biochem. Cell Biol. *40*, 2720–2738.

Krause, D.S., Ito, T., Fackler, M.J., Smith, O.M., Collector, M.I., Sharkis, S.J., and May, W.S. (1994). Characterization of murine CD34, a marker for hematopoietic progenitor and stem cells. Blood *84*, 691–701.

Leijten, J., and Khademhosseini, A. (2016). From nano to macro: multiscale materials for improved stem cell culturing and analysis. Cell Stem Cell *18*, 20–24.

Leijten, J., Chai, Y.C., Papantoniou, I., Geris, L., Schrooten, J., and Luyten, F.P. (2014). Cell based advanced therapeutic medicinal products for bone repair: keep it simple? Adv. Drug Deliv. Rev. *84*, 30–44.

Lenas, P., Moos, M., and Luyten, F.P. (2009). Developmental engineering: a new paradigm for the design and manufacturing of cell-based products. Part I: from three-dimensional cell growth to biomimetics of in vivo development. Tissue Eng. Part B Rev. *15*, 381–394.

Loh, K.M., Chen, A., Koh, P.W., Deng, T.Z., Sinha, R., Tsai, J.M., Barkal, A.A., Shen, K.Y., Jain, R., Morganti, R.M., et al. (2016). Mapping the pairwise choices leading from pluripotency to human bone, heart, and other mesoderm cell types. Cell *166*, 451–467.

Majka, M., Janowska-Wieczorek, A., Ratajczak, J., Ehrenman, K., Pietrzkowski, Z., Kowalska, M.A., Gewirtz, A.M., Emerson, S.G., and Ratajczak, M.Z. (2001). Numerous growth factors, cytokines, and chemokines are secreted by human CD34(+) cells, myeloblasts, erythroblasts, and megakaryoblasts and regulate normal hematopoiesis in an autocrine/paracrine manner. Blood *97*, 3075–3085.

Mammoto, T., Mammoto, A., Torisawa, Y.S., Tat, T., Gibbs, A., Derda, R., Mannix, R., de Bruijn, M., Yung, C.W., Huh, D., and Ingber, D.E. (2011). Mechanochemical control of mesenchymal condensation and embryonic tooth organ formation. Dev. Cell *21*, 758–769.

Moreira Teixeira, L.S., Leijten, J.C., Sobral, J., Jin, R., van Apeldoorn, A.A., Feijen, J., van Blitterswijk, C., Dijkstra, P.J., and Karperien, M. (2012). High throughput generated micro-aggregates of

chondrocytes stimulate cartilage formation in vitro and in vivo. Eur. Cell Mater. *23*, 387–399.

Morizane, A., Doi, D., Kikuchi, T., Okita, K., Hotta, A., Kawasaki, T., Hayashi, T., Onoe, H., Shiina, T., Yamanaka, S., and Takahashi, J. (2013). Direct comparison of autologous and allogeneic transplantation of iPSC-derived neural cells in the brain of a non-human primate. Stem Cell Rep. *1*, 283–292.

Nakashima, K., Zhou, X., Kunkel, G., Zhang, Z., Deng, J.M., Behringer, R.R., and de Crombrugghe, B. (2002). The novel zinc finger-containing transcription factor osterix is required for osteoblast differentiation and bone formation. Cell *108*, 17–29.

Nicks, K.M., Fowler, T.W., Akel, N.S., Perrien, D.S., Suva, L.J., and Gaddy, D. (2010). Bone turnover across the menopause transition: the role of gonadal inhibins. Ann. N. Y. Acad. Sci. USA *1192*, 153–160.

Pandit, S.K., Westendorp, B., and de Bruin, A. (2013). Physiological significance of polyploidization in mammalian cells. Trends Cell Biol. *23*, 556–566.

Pobloth, A.M., Duda, G.N., Giesecke, M.T., Dienelt, A., and Schwabe, P. (2015). High-dose recombinant human bone morphogenetic protein-2 impacts histological and biomechanical properties of a cervical spine fusion segment: results from a sheep model. J. Tissue Eng. Regen. Med. http://dx.doi.org/10.1002/term.2049.

Qi, M.C., Hu, J., Zou, S.J., Chen, H.Q., Zhou, H.X., and Han, L.C. (2008). Mechanical strain induces osteogenic differentiation: Cbfa1 and Ets-1 expression in stretched rat mesenchymal stem cells. Int. J. Oral Maxillofac. Surg. *37*, 453–458.

Roberts, S.J., van Gastel, N., Carmeliet, G., and Luyten, F.P. (2015). Uncovering the periosteum for skeletal regeneration: the stem cell that lies beneath. Bone *70*, 10–18.

Ryan, J.M. (1979). Effect of different fetal bovine serum concentrations on the replicative life span of cultured chick cells. In Vitro *15*, 895–899.

Schindeler, A., Mcdonald, M.M., Bokko, P., and Little, D.G. (2008). Bone remodeling during fracture repair: the cellular picture. Semin. Cell Dev. Biol. *19*, 459–466.

Sher, N., von Stetina, J.R., Bell, G.W., Matsuura, S., Ravid, K., and Orr-Weaver, T.L. (2013). Fundamental differences in endoreplication in mammals and *Drosophila* revealed by analysis of endocycling and endomitotic cells. Proc. Natl. Acad. Sci. USA *110*, 9368–9373.

Shields, L.B., Raque, G.H., Glassman, S.D., Campbell, M., Vitaz, T., Harpring, J., and Shields, C.B. (2006). Adverse effects associated with high-dose recombinant human bone morphogenetic protein-2 use in anterior cervical spine fusion. Spine (Phila Pa 1976) *31*, 542–547.

Stegen, S., van Gastel, N., Eelen, G., Ghesquiere, B., D'anna, F., Thienpont, B., Goveia, J., Torrekens, S., van Looveren, R., Luyten, F.P., et al. (2016). HIF-1alpha promotes glutamine-mediated redox homeostasis and glycogen-dependent bioenergetics to support postimplantation bone cell survival. Cell Metab. *23*, 265–279.

Tsuji, K., Bandyopadhyay, A., Harfe, B.D., Cox, K., Kakar, S., Gerstenfeld, L., Einhorn, T., Tabin, C.J., and Rosen, V. (2006). BMP2 activity, although dispensable for bone formation, is required for the initiation of fracture healing. Nat. Genet. *38*, 1424–1429.

Ueno, T., Kagawa, T., Mizukawa, N., Nakamura, H., Sugahara, T., and Yamamoto, T. (2001). Cellular origin of endochondral ossification from grafted periosteum. Anat. Rec. *264*, 348–357.

Wood, H.B., May, G., Healy, L., Enver, T., and Morriss-Kay, G.M. (1997). CD34 expression patterns during early mouse development are related to modes of blood vessel formation and reveal additional sites of hematopoiesis. Blood *90*, 2300–2311.

Yamamoto, H., Ngan, C.Y., and Monden, M. (2008). Cancer cells survive with survivin. Cancer Sci. *99*, 1709–1714.

Yamashita, A., Morioka, M., Yahara, Y., Okada, M., Kobayashi, T., Kuriyama, S., Matsuda, S., and Tsumaki, N. (2015). Generation of scaffoldless hyaline cartilaginous tissue from human iPSCs. Stem Cell Rep. *4*, 404–418.

Yang, L., Tsang, K.Y., Tang, H.C., Chan, D., and Cheah, K.S. (2014). Hypertrophic chondrocytes can become osteoblasts and osteocytes in endochondral bone formation. Proc. Natl. Acad. Sci. USA *111*, 12097–12102.

Zhou, X., von der Mark, K., Henry, S., Norton, W., Adams, H., and de Crombrugghe, B. (2014). Chondrocytes transdifferentiate into osteoblasts in endochondral bone during development, postnatal growth and fracture healing in mice. PLoS Genet. *10*, e1004820.

Stem Cell Reports, Volume *8*

Supplemental Information

Healing of a Large Long-Bone Defect through Serum-Free In Vitro Priming of Human Periosteum-Derived Cells

Johanna Bolander, Wei Ji, Jeroen Leijten, Liliana Moreira Teixeira, Veerle Bloemen, Dennis Lambrechts, Malay Chaklader, and Frank P. Luyten

Supplemental information
Supplemental figures

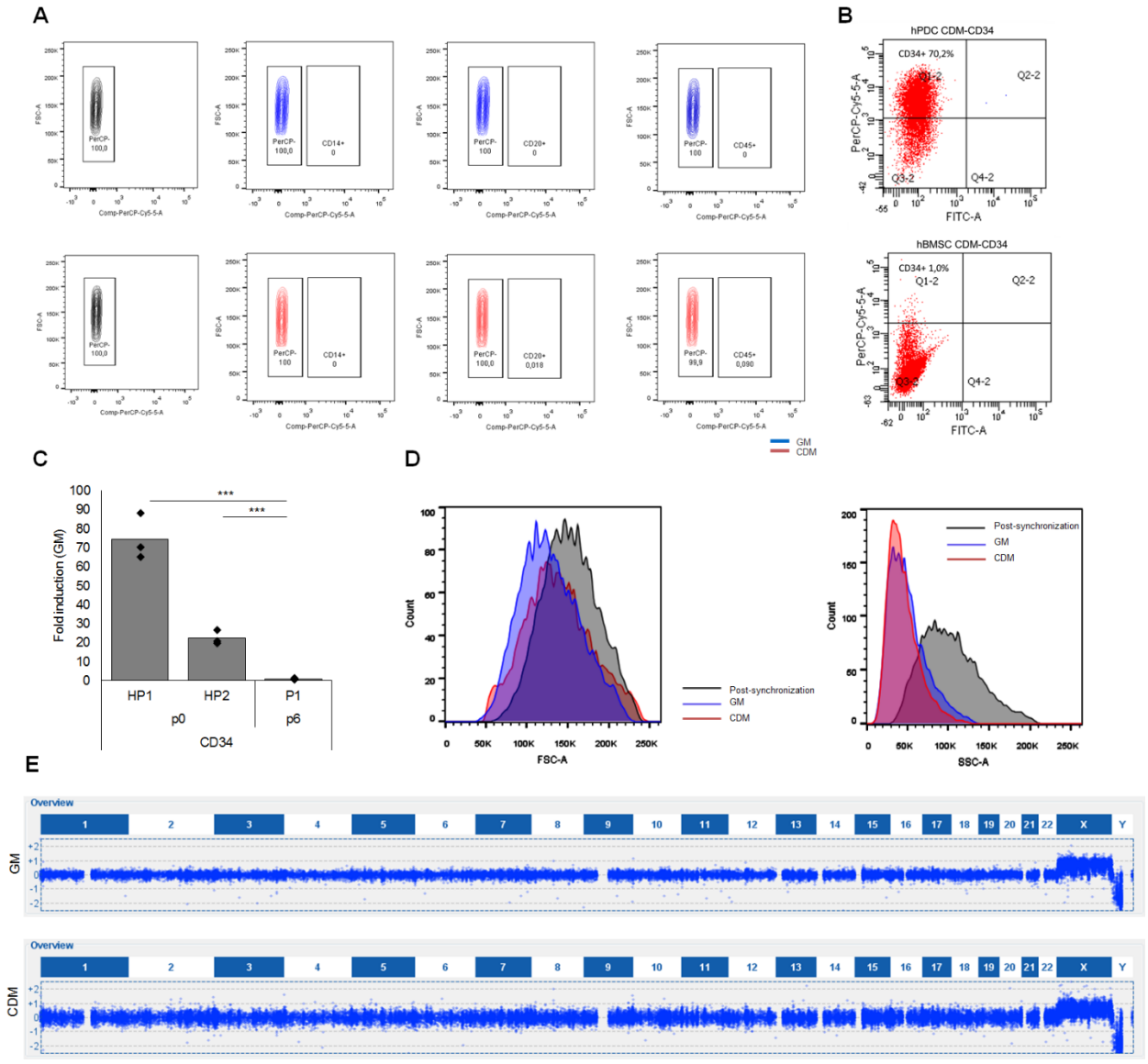

Figure S1. Serum free pre-conditioning affected hPDC phenotype. Related to Figure 1.

(**A**) Flow cytometry analysis of individual hematopoietic markers after six days of pre-conditioning in CDM or 10 % FBS. (**B**) The induced CD34 positivity by CDM pre-conditioning was specific for hPDCs and was not seen in hBMSCs. (**C**) mRNA transcript level of *CD34* in passage one (p1) hPDCs from individual donors (HP1 and HP2) and hPDCs expanded in GM to passage 6 (p6) pre-conditioned in CDM or GM. (**D**) Pre-conditioning in CDM affect cell size and granularity. (E) Karyotype analysis confirmed no significant aberrations.

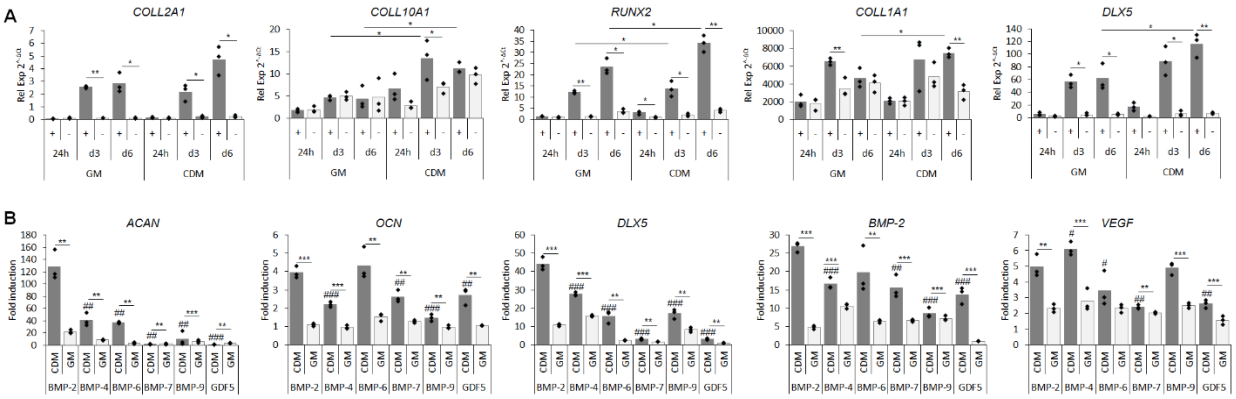

Figure S2. The serum free pre-conditioning enhanced both osteogenic and chondrogenic differentiation induced upon BMP-stimulation. Related to Figure 2.

(**A**) CDM pre-cultured cells followed by BMP-2 stimulation displayed enhanced expression of chondrogenic markers *COLL2A1*, *COLL10A1*and osteogenic markers *RUNX2* and *COLL1A1*. In addition elevated expression of transcriptional regulator *DLX5* was seen. The effect of BMP-2 in CDM pre-cultured cells was not only limited to BMP-2. (**B**) Increased expression of *ACAN*, *OCN*, *DLX5*, *BMP-2* and *VEGF* was seen in this pre-culture regimen followed by 2D stimulation of BMP-2, BMP-4, BMP-6, BMP-7, BMP-9 and GDF5. *(Statistical significance to: BMP-2: #: < 0.05, ##: < 0.01, ###: < 0.001).*

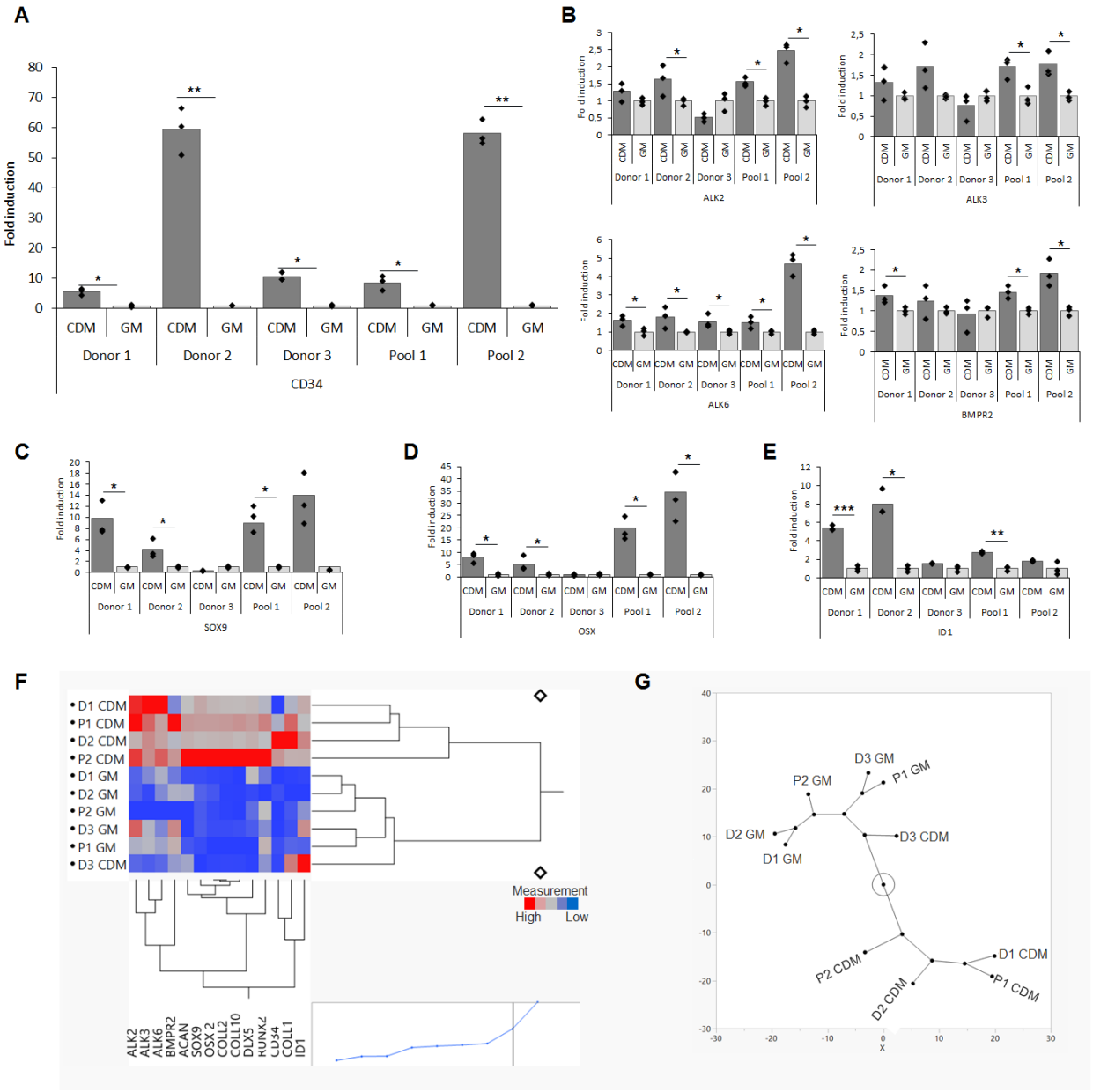

Figure S3. The improved pre-conditioning effect was confirmed in young and adult donors. Related to Figure 1 and Figure 2.

(**A**) Pre-conditioning of individual donors (D1-3) and two different pools (P1-2) of cells of different gender and ages displayed elevated CD34 expression, (**B**) as well as adapted expression level of BMP type 1 and type 3 receptors. Expression of (**C**) SOX9, (**D**) OSX and (**E**): ID1 following BMP-2 stimulation. (**F**) Cluster correlation displayed association of pre-conditioning in CDM and expression levels of marker genes. (**G**) Constellation plot over the clustered data displayed grouping of the majority of CDM pre-conditioned cell populations over individual characteristics from the specific cell populations.

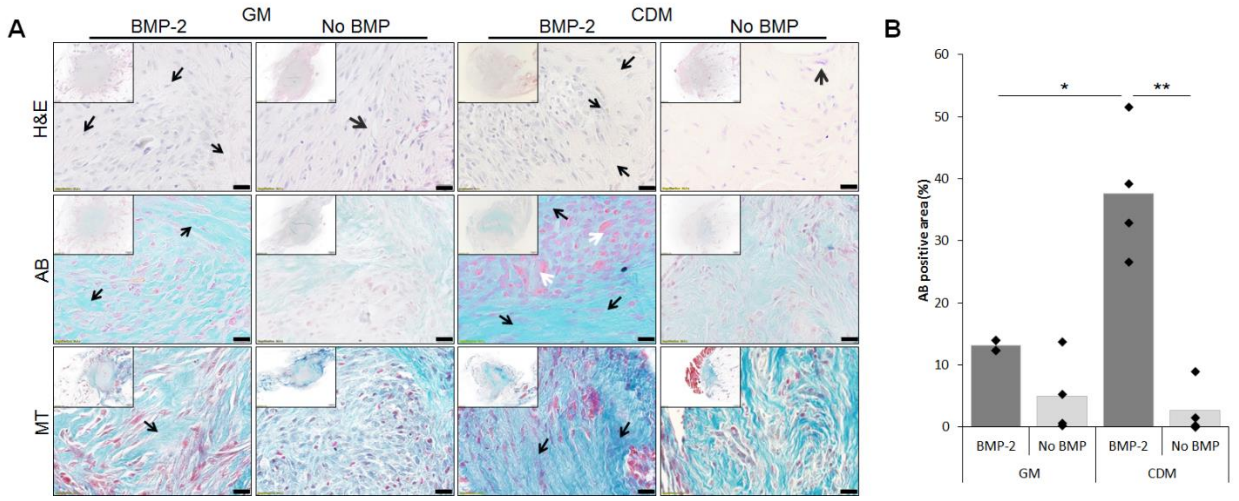

Figure S4. Serum free pre-conditioning led to enhanced GAG-production *in vivo*. Related to Figure 1 and Figure 2.

(**A**) Histology 3 weeks post subcutaneous implantation by H&E staining of *in vivo* samples displayed denser matrix formation in BMP-2 stimulated cells (black arrows) whereas more fibrous tissue were depicted in non-stimu;ated conditions (grey arrows), Alcian blue (AB) displayed cellular condensations (white arrows) surrounded by a GAG production in BMP-2 stimulated cells (black arrows) which was confirmed by Masson's Trichrome (MT) stain (black arrows). (**B**) Upon quantification of percentage of AB positive area, CDM pre-conditioning followed by BMP-2 stimulation led to elevated cartilage formation. *Scale bar: 20 µm.*

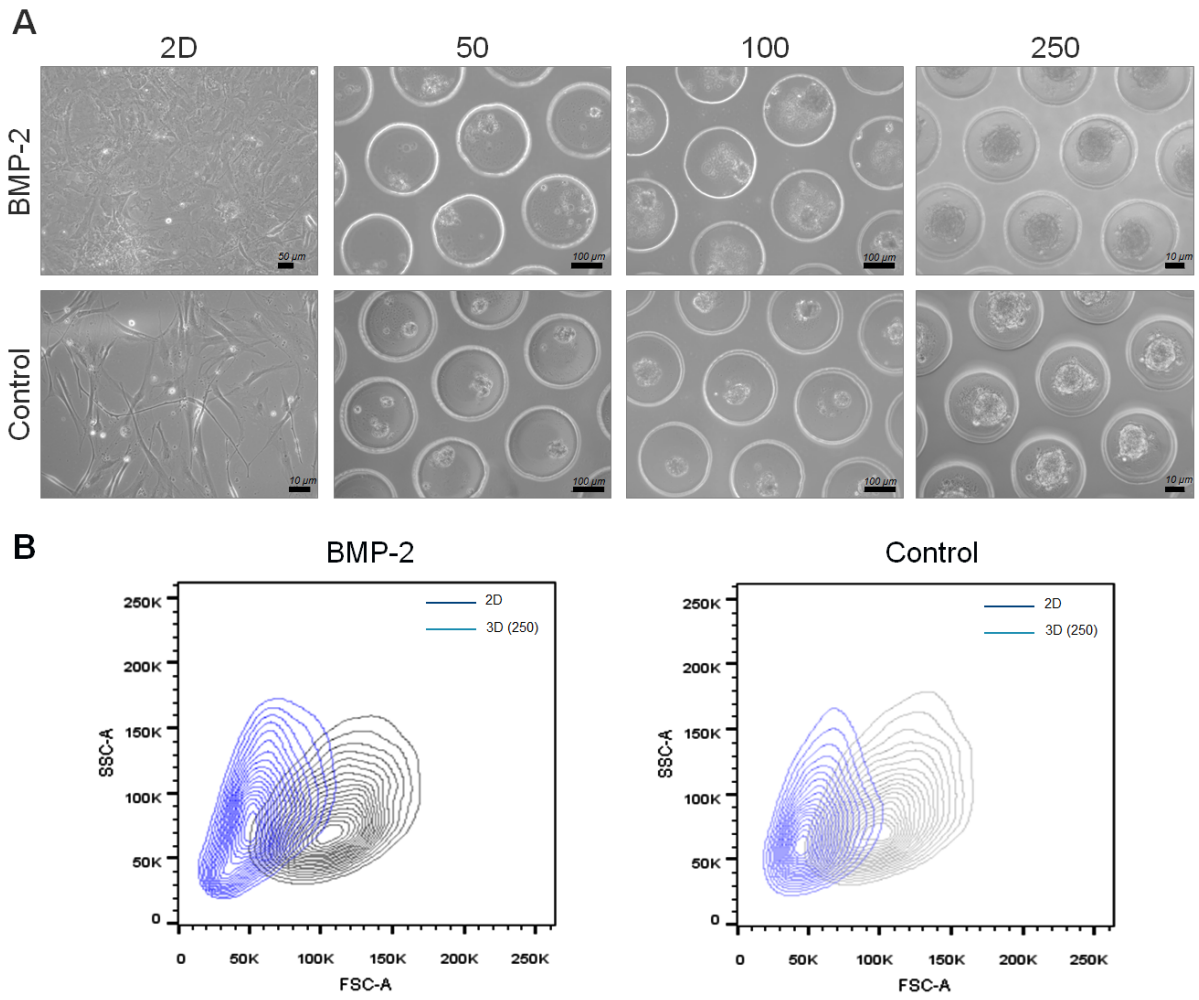

Figure S5. The number of cells per aggregate affected aggregate formation. Related to Figure 4 and Figure 5.

(**A**) Bright field images after 6 days of aggregation in cell densities of 50, 100 or 250 cells/ aggregate in the presence of or without BMP-2 displayed stable formation of aggregates of 100 and 250 cells. (**B**) Aggregation induced a decrease in cell size after disassembly of the aggregates in the presence of or without BMP-2 stimulation.

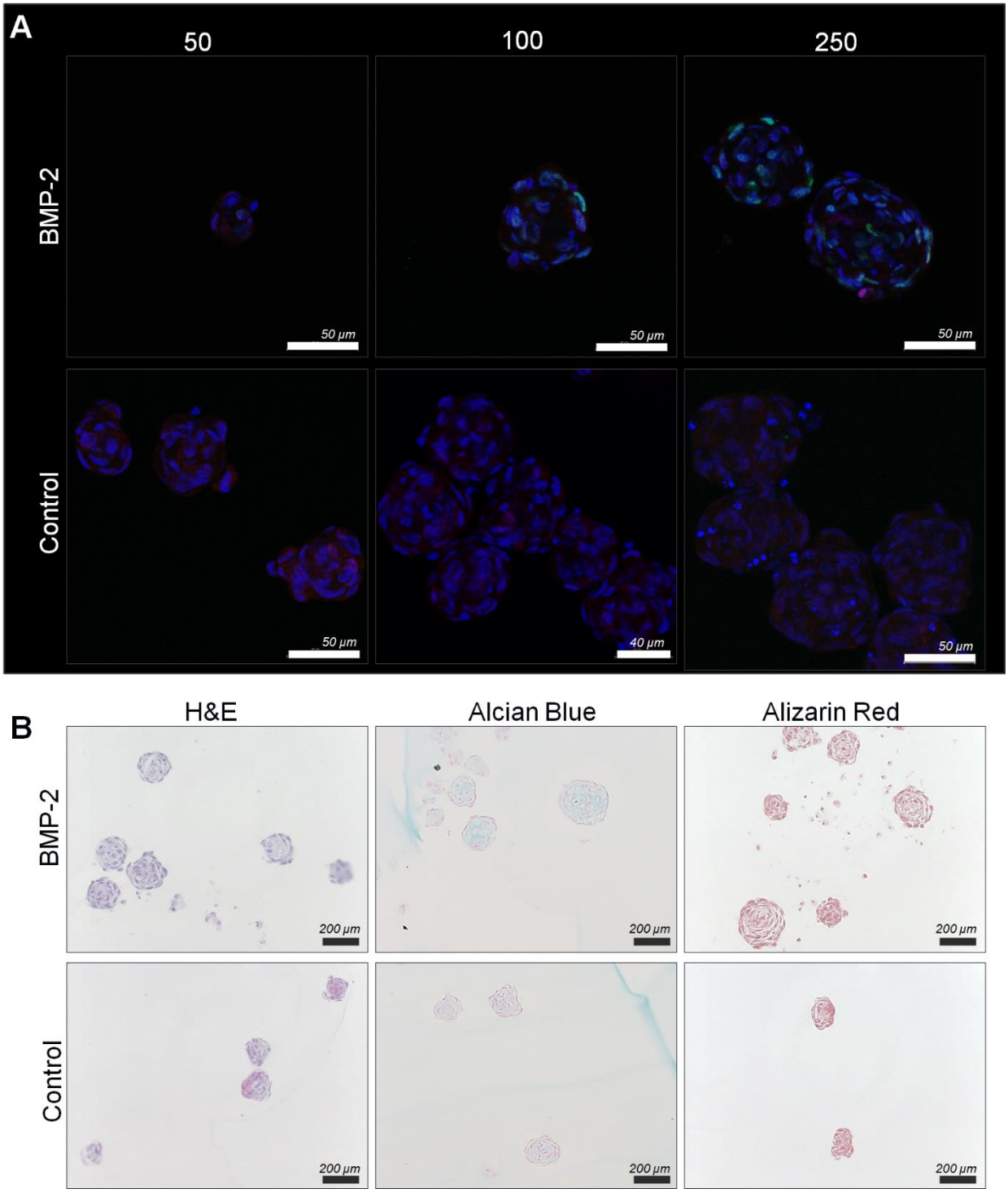

Figure S6. Aggregate size steered in vitro primed lineage specification. Related to Figure 4 and Figure 5.

(**A**) IHC for SOX9 (red), OSX (green) and DAPI (blue) on aggregates of 50, 100 or 250 hPDCs/aggregate cultured in the presence with or without BMP-2, confirm gene expression data. The results are representative of two or more independent experiments. (**B**) Histology for H&E, Alcian blue and Alizarin red on 6 days aggregated cells with and without BMP-2 stimulation displayed moderate matrix formation *in vitro*. *Unlabelled scale bar: 200 µm.*

Table S1. Primer sequences used for mRNA transcript analysis.

Gene	Forward sequence	Reverse sequence
SOX9	TGGAGACTTCTGAACGAGAGC	CGTTCTTCACCCACTTCCTC
ACAN	GTCTCACTGCCCAACTAC	GGAACACGATGCCTTTCAC
COLL2A1	GGCTTCCATTTCAGCTATGG	AGCTGCTTCGTCCAGATAGC
COLL10A1	ACGATACCAAATGCCCACAG	GTGGACCAGGAGTACCTTGC
RUNX2	CGCATTCCTCATCCCAGTAT	GCCTGGGGTCTGTAATCTGA
OSX	AGTGACCTTTCAGCCTCCAA	GGGAAAAGGGAGGGTAATCA
COLL1A1	GACGAAGACATCCCACCAAT	AGATCACGTCATCGCACAAC
OCN	GTGCAGCCTTTGTGTCCAA	GCTCACACACCTCCCTCCT
DLX5	CAGCCAAAGCTTATGCCGAC	CGGTCACTTCTTTCTCTGGCT
ID1	GGCTGTTACTCACGCCTCAAG	CCAACTGAAGGTCCCTGATGTAG
VEGF	TGCAGATTATGCGGATCAAACC	TGCATTCACATTTGTTGTGCTGTAG
BMP-2	GTATCGCAGGCACTCAGGTC	TTTTCCCACTCGTTTCTGGT
FGF2	AAAAACGGGGGCTTCTTCCT	TGTAGCTTGATGTGAGGGTCG
ALK1	ATCTGAGCAGGGCGACAC	ACTCCCTGTGGTGCAGTCA
ALK2	ATGTGACCAAGAGCCTGCAT	CGCAGGAGAGACCTTCACAC
ALK3	CAGGGCACTGTCCAGATGAT	AGCTGGGCTTTTGGAGAATC
ALK6	ATGACTCTGGGTTGCCTGTG	TCAATGGAGGCAGTGTAGGG
BMPR2	GGTTGGAAACCATCCCACTT	TGGTCCCAACAGTCTTCGAT
ACVR2a	CCGGAGATGGAAGTCACACAGCCC	TGGGGGTGGTCCTGGGTCTTGA
ACVR2b	GCTGCAGACGGACCCGTGGA	GGCCAGGCCCGGGTGTTTCA
CCNE1	GCCAGCCTTGGGACAATAATG	CTTGCACGTTGAGTTTGGGT
BIRC5	ACCAGGTGAGAAGTGAGGGA	AACAGTAGAGGAGCCAGGGA
CDK1	GGATGTGCTTATGCAGGATTCC	CATGTACTGACCAGGAGGGATAG
CD105	CACTAGCCAGGTCTCGAAGG	CTGAGGACCAGAAGCACCTC
CD34	AATGAGGCCACAACAAACATCACA	CTGTCCTTCTTAACCTCCGCACAGC

Supplemental experimental procedures

Cell culture

Isolation and *in vitro* expansion of hPDCs were carried out as previously described (De Bari et al., 2001). Cells from individual donors: donor1 (D1): 10 years female; D2: 23 years male; D3: 47 years female and two pooled populations: pool 1 (P1): 13±4.5 years and pool 2 (P2): 29±16 years, were expanded to passage six (p6) in medium containing 10 % fetal bovine serum (FBS), further referred to as (GM) as previously described (De Bari et al., 2006, Bolander et al., 2016). Cells isolated from a 43 years male (HP1) and a 16 years female (HP2) were plated and RNA was isolated after confluency was reached at the first seeding, representing p0. The P1 population was used as a representative when nothing else stated. For pre-conditioning, cells were cultured for six days in serum free chemically defined media with the removal of the growth factor cocktail, β-Glycerophosphate and lineolic acid (patent US20010039050)(Gomez-Barrena et al., 2015), further defined as serum free chemically defined media (CDM) (see below for component specification) or in GM as standard control. DNA content was measured using Quant-iT^{TM} PicoGreen$^{®}$ dsDNA assay (Invitrogen, Merelbeke, BE) according to the manufacturer's instructions (n=3). To evaluate the effect of pre-conditioning prior to differentiation, BMP-stimulation and/or aggregation was carried out for six days directly following pre-conditioning.

Detailed components in the chemically defined medium

The serum free chemically defined medium (CDM) consisted equal parts of Dulbecco's Modified Eagle Medium and HAM's F-12 (Invitrogen) supplemented with: antibiotics-antimyocotics solution (100 units/ml penicillin, 100 µg/ml streptomycin and 0.25 µg/ml amphotericin B; Invitrogen, Merelbeke, BE), 5 µg/ml ITS^{TM} PREMIX (BD Biosciences), 2 µg/ml L-α-Phosphatidylethanolamine (Jena Bioscience), 1x10^{-4} M α-ketoglutaric acid, 1.25 µg/ml Taurine, 0,25 U/ml Cerulosplasmin, 5 µg/ml Cholesterol, 10 µg/ml L-gluthatione reduced, 1,25 µg/ml Taurine, 9x10^{-7} M D-α-tochopherol succinate, 50 µg/ml L-ascorbic acid 2 sulphate, 1,6x10^{-9} M 3,3',5-Triiodo-L-thyronine sodium salt, 1x10^{-9} M Hydrocortisone and 5x10^{-10} M Parathyroid hormone (Sigma-Aldrich).

Flow cytometry

Flow cytometry was performed to characterize the expression of stemness markers on human periosteal cells by using human MSC Phenotyping kit (130-095-198, Miltenyi Biotec, Leiden, NL). Individual marker expression on hPDCs was characterized by staining the cells with human specific CD14-PerCP, CD20-PerCP, CD-34 PerCP-Vio700, CD45-PerCP, CD105-PE (130-098-072, 130-098-077, 130-097-915, 130-098-145, 130-098-906, Miltenyi Biotec). The extracellular staining was performed according to manufacturer's instructions. In brief, cells were mixed with MSC Phenotyping Cocktail or individual antibodies and incubated in dark at 4°C. After staining, the cells were washed and analysed using BD FACS Canto^{TM}cell analyser (BD Biosciences, Erembodegem, BE) with FlowJo V10 software. The number of cell surface receptors expressed per cell was quantified using BD QuantiBRITE^{TM}-Phycoerythrin beads (BD Biosciences, San Jose, CA),) as previously described (Pannu et al., 2001).

Cell separation

Separation of CD34^{+} cells was performed with a COLiso Magnetic Separation Kit-Human CD34^{+}Cells according to the manufacturers' instructions (K10134, ProMab Biotechnologies, Richmond, US). Upon separation, 94% purity of CD34^{+} cells of which 100% were CD14^{-}, CD20^{-} and CD45^{-}, as confirmed by flow cytometry.

Karyotype analysis

Genomic DNA was extracted using the QIAamp DNA Blood Mini QIAcube Kit on the Qiacube robotic workstation according to the manufacturer's instructions. Array analysis was performed using the 8x 60K CytoSure ISCA v2 microarray (AMADID 020040, Oxford Gene Technology, OGT, Oxford, UK). Genomic DNA was labeled for 2 hours using the CytoSure Labelling Kit (Oxford Gene Technology). The sample was labeled with Cy5 and hybridized versus Cy3-labeled sex-matched reference DNA. Hybridization was performed for minimum 16 hours in a rotator oven (SciGene, CA, US) at 65 °C. Washing of arrays was performed using Agilent wash solutions with a Little Dipper Microarray Processor (SciGene). Arrays were scanned using an Agilent microarray scanner at 2-µm resolution, followed by calculation of signal intensities using Feature Extraction software (Agilent Technologies).Visualization of results and data analysis were performed using the CytoSure Interpret Software (Oxford Gene Technology) and the circular binary segmentation algorithm. Quality control metrics are monitored with CytoSure Interpret software (Oxford Gene Technology).

In vitro BMP-stimulation and evaluation

Pre-conditioned cells were seeded at a cell seeding density of 10 000 cells/cm^2 followed by stimulation in CDM or GM containing 10% FBS supplemented with 100ng/ml BMP-2 (Medtronics, Minneapolis, Minnesota, US), BMP-4, -6, -7, -9 or GDF6 (Peprotech, London, UK). To investigate *in vitro* differentiation, samples were collected for DNA quantification and Alkaline phosphatase (ALP) activity was measured using a commercial kit (Kirkegaard & Perry, Guilford, UK) normalized to DNA content. mRNA analysis were performed as previously described (Bolander et al., 2016), primer sequences are listed in supplementary table 1. To investigate nuclear translocation of downstream signalling molecules, Western blot analysis was performed. After 6 days of BMP-2 stimulation, cells were homogenised in Cell extraction buffer containing 0.3 M Phenylmethanesulfonyl fluoride and Protease Inhibition Cocktail (Sigma-Aldrich, Bornem, BE). Protein concentration was determined using the Pierce BCA Protein Assay Kit (Thermo Scientific) according to manufacturer's instructions. Equal quantities of protein was loaded on NuPAGE 4-12 % Bis-Tris gels (Invitrogen) and electrophoresed to separate proteins according to size. These proteins were subsequently transferred to a Polyvinylidene fluoride membrane by wet transfer for further analysis. Primary antibodies were diluted according to the manufacturer`s instructions: rabbit monoclonal Phospho-p44/42 MAPK (Erk1/2) (Thr202/Tyr204) (197G2)(43775), rabbit polyclonal p44/42 MAPK (Erk1/2)(9102), rabbit monoclonal Phospho-p38 MAPK (Thr180/Tyr182) (12F8)(4631), rabbit polyclonal p38 MAPK(9212), rabbit polyclonal Phospho-SMAD1 (Ser463/465)/SMAD5 (Ser463/465)/SMAD8 (Ser426/428)(9516), rabbit polyclonal SMAD1(6944), rabbit polyclonal SMAD2/3 (5678)(Cell Signalling Technology- BIOKÉ, Leiden, NL), mouse monoclonal Anti-Active-β-Catenin (05-665)(EMD Millipore, Overijse, BE), goat polyconal Phospho-SMAD2/3 (Ser423/425) (sc-11769)(Santa Cruz Biotechnology, Inc, Heidelberg, DE). Glyceraldehyde-3-phosphate dehydrogenase (GAPDH) mouse monoclonal (Abcam) was used to assess equal loading of proteins. HRP-conjugated secondary antibodies were used at a dilution of 1:2000 (Jackson, Pennsylvania, US) and images were developed by a LAS3000 Imaging System (FUJI) following the application of SuperSignal® West Femto reagent (Thermo Scientific, Illnois, US). Densitometry analysis was performed using Biorad Quantity One software.

3D Microwell fabrication and cell aggregation

Fabrication of a microwell platform allowing for high throughput production of microaggregates with controlled cell density per aggregate was performed as previously described (Leijten et al., 2016). To seed hPDCs in aggregates containing 50, 100 or 250 cells/aggregate, the microwells were covered in 2 ml of CDM containing 100.000, 200.000 or 250.000 cells, respectively, allowing for the formation of 1000 aggregates/well. The stimulatory effect of aggregation in combination with or without BMP-2 was investigated by flowcytometry, mRNA transcript analysis and IHC.

In vivo implantation

Pre-conditioned and 2D stimulated cells or aggregates were washed and collected and 1*10^6 cells were encapsulated in a 100 µl Collagen type 1 gel, (5 mg/mL, BD Biosciences) and implanted subcutaneously in NMRI$^{nu/nu}$ mice. In addition, BMP-2 stimulated monolayer cultures of hPDCs followed by 24h aggregation in the absence of BMP-2 were included to study the effect of separate stimulation of BMP-2 and aggregation. Explants were harvested at 1, 3 and 6 weeks post implantation and qualitatively analysed by histology and IHC, for all ectopic conditions n=4. For orthotopic evaluation, CDM pre-conditioned hPDC were stimulated as aggregates in the presence of BMP-2 for 6 days. Subsequently after washing, the aggregates were collected and implants of 30 µl collagen type 1 gels (5 mg/mL, BD Biosciences) containing 1200 aggregates/gel were prepared. Subsequently, a critical size 4 mm long bone defect was created in the right hind tibiae of NMRI$^{nu/nu}$ mice, allowing to examine the regenerative bone-forming potential of the *in vitro* prepared construct as previously described (van Gastel et al., 2014). In total, 6 constructs were implanted, 4 for week 8, 2 for week 4 and 2 for week 2. As control for the critical defect, 5 fractures were made were one was excluded from the study due to surgical error with remnants of bone spicules in the fracture. At harvest, samples were fixated using 2% paraformaldehyde for 12 h. Explants from the orthotopic model were analysed by *ex vivo* nano-CT as previously described (Bolander et al., 2016), and samples were processed for IHC and histology.

Immunohistochemistry

To further identify cell differentiation, IHC was performed by dual immunohistochemistry (IHC) for SOX9 (NB100-304, NovusBiologicals, Abingdon, UK) and OSX (MAB7547, R&D Systems, Abingdon, UK). As secondary antibodies: Alexa 488 anti-mouse, (1:500) together with Biotinylated SP-conjugated goat anti rabbit (1:500) were used followed by incubation with Streptavidin Alexa 555 (1:500) (Jackson ImmunoResearch, Philadelphia, US) and DAPI (1:2500). Microscopic analysis was performed by confocal imaging using a FluoView FV1000 setup (Olympus) and visualized by Z-stacking of images obtained with a UPLSAPO 60x oil objective at 0.265 um x 0.265 um pixel size, and images acquired in z-direction were separated by a distance of 1.83 um. To identify *in vivo* tissue development, a

rabbit Phospho-SMAD1 (Ser463/465)/ SMAD5 (Ser463/465)/ SMAD8 (Ser465/467) antibody (Cell signalling, Leiden, NL), mouse Aggrecan monoclonal antibody to N-terminal neoepitope (DIPEN) (clone BC4) (1042002, MD Bioscience, Switzerland), rabbit polyclonal Anti-S100 (Z0311, Dako, Heverlee, BE) and rabbit polyclonal Anti-Ihh antibody - N-terminal (ab80191, abcam, Cambridge, UK) were used according to the manufacturers' instructions. Contribution to *de novo* formed tissue by implanted cells were investigated using a human specific primary anti-OCN guinea pig antibody (a generous gift from Dr. E. Van Herck, Legendo, KU Leuven, BE) which does not cross-react with mouse OCN (De Bari et al., 2006). As secondary antibodies, peroxidase-conjugated goat anti-rabbit, -mouse, or -guinea pig (Jackson ImmunoResearch) were used. For non-fluorescent IHCs, 3,30-diaminobenzidine (Sigma-Aldrich) were used as a chromogenic substrate and hematoxylin as counterstain. Tissue sections were visualized with an inverted microscope (IX83-P22F, Olympus).

Histology

To visualize glycosaminoglycans, samples were stained with acidic Alcian Blue (pH=1, Merck, Damstadt, DE) and counterstained with nuclear fast red (Vector Laboratories, Brussels, Belgium). General matrix staining was visualized using hematoxyline (Sigma-Aldrich) and eosin staining (Klinipath, Duiven, NL). Masson's Trichrome staining was performed to visualize immature and mature bone tissue by immersing sections in Weigerts iron hematoxylin solution, subsequently stained with ponceau-acid fuchsin solution (0.5% ponceau BS, 0.5% acid fuchsin in 10% acetic acid) followed by differentiation in 5% phosphomolybdic acid 5% phosphotungstic acid solution. The sections were then transferred directly to Mason's green solution (Klinipath, Olen, BE) before differentiation in 1% acetic acid. TRAP stain was performed to localize osteoclast activity as previously described (Bolander et al., 2016). Histological sections were visualized using an inverted imaging setup (IX83-P22F, Olympus).

Histomorphometry

For semi-quantitative analysis, stained tissue sections were imaged for an overview or at four defined locations per section and used as a representative. ImageJ software was used for quantification of positive staining and scanned images from 3 sections per explants were utilized for an average value. The color threshold was adjusted to depict the positive areas by defining minimum and maximum values for each color on control samples and an in-house developed MatLab code was used to quantify the positive area normalised to the total area.

Investigation of endogenous BMP production

Endogenous production of BMP-2 was analysed by a human BMP-2 ELISA development kit (Peprotech) in conditioned media from 6 days *in vitro* stimulated conditions. Fresh stimulation media was used as baseline. The ELISA was performed according to the manufacturer's instructions.

Statistical analysis

Data are expressed as individual data points with bars representing the average value. Statistical evaluation was determined using a non-paired unequal variance student t-test to compare between independent groups. Statistical significance is indicated on all graphs as follows between conditions: *:$p < 0.05$, **: $p < 0.01$, ***: $p< 0.001$ if nothing else is stated. Results are conducted from at least 3 independent experiments, n=3 for *in vitro* data and n=/>4 for *in vivo* experiments. Hierarchical clustering was performed using Ward's method in JMP® 10 (SAS Institute Inc., Cary, NC).

Supplemental results

The improved effect of serum free pre-conditioning was not age or gender dependent

The effect of the serum free pre-conditioning was confirmed in young and adult donors (D1-3) as well as in two cell pools with a different age average (P1-2) in which an elevated CD34 expression was correlated to enhanced expression of BMP-receptors (Figure S3A and B). In addition, BMP-2 stimulation induced elevated differentiation confirmed by *SOX9*, *OSX* and *ID1* expression (Figure S3C-E). Importantly, with ID1 expression as an example, the coefficient of variance was a 5-, 2-, 8-, 6- and 14-fold higher in serum conditions for the D1-P2 populations, respectively. Interestingly, the effect of the pre-conditioning led to a specific cluster correlation depending on the pre-conditioning (Figure S3F). A constellation plot displayed that pooled cell populations can function as a representative for individual donors, since the improved potential was independent of gender and age, but potentially affected by combined donor characteristics (Figure S3G).

Enhanced in vitro differentiation leads to elevated cartilaginous matrix deposition in vivo

To investigate the *in vivo* effect of the pre-conditioning regimen, BMP-2 stimulated cells were encapsulated in a COLL1 gel and implanted ectopically for three weeks to evaluate the potency of the cells to produce cartilage. H&E staining displayed denser staining in BMP-2 stimulated explants, which was further elevated in CDM pre-conditioned cells (black arrows) (Figure S4A). Fibrous tissue was mainly depicted in non-stimulated cells (grey arrows). The deposition of a glycosaminoglycan (GAG)-rich matrix by Alcian Blue (AB) staining demonstrated the presence of GAGs in BMP-2 treated implants (black arrows). Image quantification corroborated denser stain in CDM pre-conditioned cells followed by BMP-2 stimulation combined with cellular condensations (white arrows) (Figure S4B). The AB staining was further confirmed by Masson's Trichrome (MT) with denser areas indicated by black arrows (Figure S4B). These findings indicate that the potent response seen *in vitro* was also reflected *in vivo*.

Supplemental references

BOLANDER, J., JI, W., GERIS, L., BLOEMEN, V., CHAI, Y. C., SCHROOTEN, J. & LUYTEN, F. P. 2016. The combined mechanism of bone morphogenetic protein- and calcium phosphate-induced skeletal tissue formation by human periosteum derived cells. *Eur Cell Mater,* 30**,** 11-25.

DE BARI, C., DELL'ACCIO, F. & LUYTEN, F. P. 2001. Human periosteum-derived cells maintain phenotypic stability and chondrogenic potential throughout expansion regardless of donor age. *Arthritis Rheum,* 44**,** 85-95.

DE BARI, C., DELL'ACCIO, F., VANLAUWE, J., EYCKMANS, J., KHAN, I. M., ARCHER, C. W., JONES, E. A., MCGONAGLE, D., MITSIADIS, T. A., PITZALIS, C. & LUYTEN, F. P. 2006. Mesenchymal multipotency of adult human periosteal cells demonstrated by single-cell lineage analysis. *Arthritis Rheum,* 54**,** 1209-21.

GOMEZ-BARRENA, E., ROSSET, P., LOZANO, D., STANOVICI, J., ERMTHALLER, C. & GERBHARD, F. 2015. Bone fracture healing: cell therapy in delayed unions and nonunions. *Bone,* 70**,** 93-101.

LEIJTEN, J., TEIXEIRA, L. S., BOLANDER, J., JI, W., VANSPAUWEN, B., LAMMERTYN, J., SCHROOTEN, J. & LUYTEN, F. P. 2016. Bioinspired seeding of biomaterials using three dimensional microtissues induces chondrogenic stem cell differentiation and cartilage formation under growth factor free conditions. *Sci Rep,* 6**,** 36011.

PANNU, K. K., JOE, E. T. & IYER, S. B. 2001. Performance evaluation of QuantiBRITE phycoerythrin beads. *Cytometry,* 45**,** 250-8.

VAN GASTEL, N., STEGEN, S., STOCKMANS, I., MOERMANS, K., SCHROOTEN, J., GRAF, D., LUYTEN, F. P. & CARMELIET, G. 2014. Expansion of murine periosteal progenitor cells with fibroblast growth factor 2 reveals an intrinsic endochondral ossification program mediated by bone morphogenetic protein 2. *Stem Cells,* 32**,** 2407-18.